Lysosomal Cholesterol Hydrolysis Couples Efferocytosis to Anti-Inflammatory Oxysterol Production

Manon Viaud[1], Stoyan Ivanov[1], Nemanja Vujic[3], Madalina Duta-Mare[3], Lazaro-Emilio Aira[1], Thibault Barouillet[2], Elsa Garcia[1], Francois Orange[4], Isabelle Dugail[5], Isabelle Hainault[6], Christian Stehlik[7], Sandrine Marchetti[1], Laurent Boyer[1], Rodolphe Guinamard[1], Fabienne Foufelle[6], Andrea Bochem[8], Kees G Hovingh[9], Edward B Thorp[7], Emmanuel L Gautier[5], Dagmar Kratky[3], Paul Dasilva-Jardine[10], Laurent Yvan-Charvet[1]

[1]Institut National de la Santé et de la Recherche Médicale (Inserm) U1065, Université Côte d'Azur, Centre Méditerranéen de Médecine Moléculaire (C3M), Atip-Avenir, Fédération Hospitalo-Universitaire (FHU) Oncoage, 06204 Nice, France; [2]Acquire Innovation Ltd, Coliemore House, Coliemore Road, A96A8D5 Dakley CO. Dublin, Ireland; [3]Gottfried Schatz Research Center for Cell Signaling, Metabolism & Aging, Molecular Biology and Biochemistry, Medical University of Graz, Graz, Austria; [4]UFR Sciences, Faculté des Sciences de l'Université de Nice- Sophia Antipolis, Parc Valrose, 28 avenue Valrose, 06108 Nice, France; [5]Institut National de la Santé et de la Recherche Médicale (INSERM) UMR_S 1166, Pierre & Marie Curie University, ICAN Institute of Cardiometabolism & Nutrition, Hôpital de la Pitié, Boulevard de l'Hôpital, 75006 Paris, France; [6] Institut National de la Santé et de la Recherche Médicale (Inserm) UMRS 1138, Centre de Recherche des Cordeliers, F-75006, Paris, France; [7]Feinberg Cardiovascular Research Institute, Department of Pathology, Feinberg School of Medicine, Northwestern University, Chicago, IL 60611; [8]Cardiology, Academic Medical Center, Amsterdam, the Netherlands; [9] Department of Vascular Medicine, Academic Medical Center, Amsterdam, The Netherlands, and; [10]Staten Biotechnology, 5 TransistorWeg Nijmegen, The Netherlands.

*M.V. and S.I. contributed equally to this work

Running title: LIPA and Efferocytic Inflammation

Subject Terms:
Inflammation
Lipids and Cholesterol
Metabolism

Address correspondence to:
Dr. Laurent Yvan-Charvet
Institut National de la Santé et de la Recherche Médicale (Inserm) U1065
Université Côte d'Azur
Centre Méditerranéen de Médecine Moléculaire (C3M)
Atip-Avenir
Fédération Hospitalo-Universitaire (FHU) Oncoage
06204 Nice
France
yvancharvet@unice.fr

In February 2018, the average time from submission to first decision for all original research papers submitted to *Circulation Research* was 12 days.

ABSTRACT

***Rationale*:** Macrophages face a substantial amount of cholesterol following the ingestion of apoptotic cells and the lysosomal acid lipase (LIPA) has a major role in hydrolyzing cholesteryl esters in the endocytic compartment.

***Objective*:** Here, we directly investigated the role of LIPA-mediated clearance of apoptotic cells both in vitro and in vivo.

Methods and Results: We show that LIPA inhibition causes a defective efferocytic response due to impaired generation of 25-OHC and 27-OHC. Reduced synthesis of 25-OHC after LIPA inhibition contributed to defective mitochondria associated membrane (MAM) leading to mitochondrial oxidative stress-induced NLRP3 inflammasome activation and caspase 1-dependent Rac1 degradation. A secondary event consisting of failure to appropriately activate liver X receptor-mediated pathways led to mitigation of cholesterol efflux and apoptotic cell clearance. In mice, LIPA inhibition caused defective clearance of apoptotic lymphocytes and stressed erythrocytes by hepatic and splenic macrophages, culminating in splenomegaly and splenic iron accumulation under hypercholesterolemia.

***Conclusions*:** Our findings position lysosomal cholesterol hydrolysis as a critical process that prevents metabolic inflammation by enabling efficient macrophage apoptotic cell clearance.

Keywords:
Lysosomal acid lipase (LIPA), oxysterols, efferocytosis, inflammation, macrophage, cholesterol.

Nonstandard Abbreviations and Acronyms:

AL	Apoptotic lymphocytes
ATMs	Adipose tissue macrophages
CESD	Cholesteryl Ester Storage Disease
E	Endoplasmic reticulum
GRP78	78 kDa glucose-regulated protein
GWAS	Genome-wide association studies
HDL	High-density lipoprotein
KC	Kupffer cells
LAP	Microtubule-associated protein 1A/1B-light chain 3 (LC3)-associated phagocytosis
LDL	Low-density lipoprotein
LIPA	Lysosomal acid lipase
LPS	Lipopolysaccharide
MAM	Mitochondria associated membrane
NLRP3	NOD-like receptor family, pyrin domain containing
NOX2	Nicotinamide adenine dinucleotide phosphate (NADPH) oxidase 2
OCR	Oxygen consumption rate
OXPHOS	Oxidative phosphorylation
PMs	Peritoneal Macrophages
Rac1	Ras-related C3 botulinum toxin substrate 1
RBC	Red blood cell
ROS	Reactive oxygen species
RPMs	Red pulp macrophages
TFEB	Transcription factor E-box

INTRODUCTION

Macrophages regulate tissue homeostasis through the uptake and catabolism of plasma lipoproteins, thus avoiding ectopic lipid deposition.[1,2] Tissue integrity also results from the efficient efferocytic capacity of macrophages to prevent the leakage of immunogenic peptides and lipid contents from dying cells.[3,4] When macrophages ingest modified lipoproteins or apoptotic cells, they increase their cellular contents and metabolic load. Excess cholesterol delivered to macrophages by these pathways must be processed within the lysosome and then re-esterified for storage leading to noncytotoxic macrophage foam cell formation.[5-7] Excess cholesterol can also be exported to extracellular acceptors via cholesterol efflux pathways to prevent the cytotoxic effects associated with elevated free cholesterol within the endoplasmic reticulum (ER) or the formation of cholesterol crystals within the lysosome.[8,9] The efflux of cholesterol is governed by liver X receptors (LXRs), which are members of the nuclear receptor superfamily that not only sense an excess of cholesterol but also regulate genes involved in anti-inflammatory responses.[7,10]

Lysosomal acid lipase (LIPA) is a unique acid hydrolase enzyme that breaks down fatty material within the lysosomal compartment of cells. In humans and mice, LIPA deficiency is associated with multiple complications, including severe dyslipidemia, abnormal liver function, hepatomegaly, splenomegaly and accelerated atherosclerosis due to the accumulation of fatty deposits and the formation of pathogenic macrophage foam cells.[11,12] Interestingly, myeloid cell-specific re-expression of LIPA in LIPA-deficient mice corrects most of their inflammatory and tissue pathogenic phenotypes.[13] This finding suggests that macrophage LIPA expression plays a non-redundant role in tissue lipid homeostasis by preventing metabolic inflammation. However, the underlying molecular mechanisms that drive this inflammation remain to be elucidated.

In macrophages, LIPA hydrolyzes not only fatty materials upon CD36 scavenger receptor-mediated endocytosis to promote mitochondrial fatty acid oxidation,[14] but also cholesteryl esters upon the fusion of lipid droplets with lysosomes to support free cholesterol efflux, a process termed lipophagy.[15] This illustrates the pivotal role of LIPA at the interface of different catabolic pathways. Of note, the unabated uptake of modified lipoprotein-derived cholesterol and defective autophagy have been linked to sterile inflammation as a consequence of cholesterol crystal formation within macrophage lysosomes, promoting the assembly of the NLRP3 inflammasome and activation of caspase-1.[16,17] Although, a protective role of LIPA in macrophages during acute parasitic infection has recently emerged,[14] the contribution of LIPA-dependent processing of cholesteryl esters in sterile inflammation remains elusive.

To test the causal relationship between lysosomal cholesterol processing and macrophage function, we explored the role of LIPA after engulfment of apoptotic cells. We report here that LIPA is critical for efficient efferocytosis. These effects were mediated not by defective LC3-associated phagocytosis-engaged phagosome (LAPosome) formation or lysosomal dysfunction. We rather report that LIPA controls the generation of 25- and 27- hydroxycholesterol (OHC). Reduced 25-OHC after LIPA inhibition contributed to defective mitochondria associated membrane (MAM)-dependent mitochondrial metabolic repurposing leading to activation of the NLRP3 inflammasome after efferocytosis. Activation of the inflammasome subsequently promoted defects in Rac1-dependent phagocytic cup formation. Reduced 25- and 27-OHC also contributed to dampen LXR activation causing mitigation of cholesterol efflux and apoptotic cell clearance. In vivo experiments confirmed that LIPA inhibition led to defective clearance of apoptotic cells and stressed erythrocytes by splenic and hepatic macrophages. This process culminated in splenomegaly and splenic iron accumulation under hypercholesterolemic conditions. Our data highlight that LIPA is integral to macrophage efferocytic response, and they provide a framework for understanding the contribution of LIPA to chronic inflammation.

METHODS

All data and methods used in the analysis and materials used to conduct the research will be made available to any researcher for the purpose of reproducing the results or replicating the procedures.

All data, methods, and materials are available on personal request at the University Côte d'Azur, Centre Méditerranéen de Médecine Moléculaire (L.Y.C).

An expanded Methods section is available in the Online Data Supplement

Animals and treatments.

WT and Ldlr$^{-/-}$ mice in a C57BL6/J background were obtained from the Janvier Lab (Saint Berthevin, France) and fed a normal chow diet. Hyperlipidemia was induced by feeding the mice with a Western diet (TD88137, Ssniff) for 12 weeks. Two weeks before the end of the study, mice were challenged with subcutaneous injections every two days of 20mg/kg lalistat (Enamine) solubilized in 0,5% methylcellulose 0,1% Tween 20 or with control solution**.** Mice were sacrificed one day after the last injection. All animals procedures were approved by the Institutional Animal Care and Use Committee of the French Ministry of Higher Education and Research and the Mediterranean Center of Molecular Medicine (Inserm U1065) and were undertaken in accordance with the European Guidelines for Care and Use of Experimental Animals. Animals had free access to food and water and were housed in a controlled environment with a 12-hour light–dark cycle and constant temperature (22°C).

RESULTS

Optimal clearance of apoptotic cells depends on LIPA.

We first made the observation that opposing regulation of LIPA activity occurred between classical (LPS) and alternative (IL-4) macrophage activation, and this correlated with the efferocytic capacity of these cells (Fig. 1A). Thus, we examined whether LIPA could impact efferocytosis in human THP-1 macrophages. Efferocytosis was analyzed 30 minutes after exposure to apoptotic Jurkat cells in LIPA deficient cells (LIPA knockdown using siRNA or lentiviral ShRNA particles (Online Fig. IA)) or LIPA overexpressing cells (Ovex, using stable transfection (Online Fig. IB)). Remarkably, LIPA expression modulated optimal engulfment of apoptotic cells as shown after knockdown or overexpression (Fig. 1B). These efferocytic responses paralleled BODIPY-neutral lipid stainings in both LIPA-deficient and LIPA-overexpressing THP-1 macrophages 30 minutes following ingestion of apoptotic cells (Fig. 1C). LIPA inhibition was next achieved with lalistat. A time course experiment showed that the efferocytic index was unaffected by lalistat 3 and 6 hours post-efferocytosis in THP-1 macrophages but was significantly reduced by 46% 24 hours after efferocytosis (Fig. 1D-E). Consistently, reduced phagocytic capacity was also observed in LIPA deficient murine bone marrow-derived macrophages and lalistat treatment did not show any additive effects in these cells (Online Fig. IC). These results reveal that LIPA inhibition initiates a sequential cascade of events that leads to impaired efferocytic response. Importantly, quantification of BODIPY staining in a time-course experiment revealed that neutral lipid accumulation preceded defects observed on efferocytosis after LIPA inhibition both in THP-1 macrophages (Fig. 1F) and murine primary macrophages (Online Fig. ID). Thus, LIPA-dependent clearance of apoptotic cells is most likely the consequence on how efferocytes initially handle cholesterol, the main neutral lipid in macrophages.

LIPA controls lysosomal cholesterol trafficking during efferocytosis.

To better comprehend the mechanism by which LIPA modulates the efferocytic response, we performed an assay to follow the diffusion of cholesterol within intracellular compartments. Human THP-1 macrophages that had been cultured for 1 hour after the ingestion of [^{3}H]-cholesterol-prelabeled apoptotic Jurkat cells were fractionated by sucrose step gradient, and cellular fractions were assayed for [^{3}H]-cholesterol levels. The accumulation of cholesterol was observed 1 hour after efferocytosis in the high-density membrane fraction (enriched in endosomes and lysosomes) and in the plasma membrane fraction of lalistat-treated efferocytes (Fig. 1G). In contrast, reduced cholesterol content in high-density membrane fraction was observed 1 hour after the ingestion of [^{3}H]-cholesterol-prelabeled apoptotic Jurkat cells in LIPA overexpressing cells (Online Fig. IE). As expected, cholesteryl esters accumulated in the high-density membrane fraction after LIPA inhibition and to some extent in the plasma membrane fraction (Online Fig. IF). At this time point, there was no significant difference in the amount of cholesterol diffusing in the Golgi but less diffusion of free cholesterol occurred in the ER fraction in lalistat-treated THP-1 macrophages compared to control cells (Fig. 1G and Online Fig IF). Consistent with the accumulation of cholesteryl esters rather than free cholesterol after LIPA inhibition, transmission electron microscopy revealed only sparse cholesterol crystal formation in lalistat-treated THP-1 macrophages (1 identified among more than 400 visualized lysosomes with similar structures) (Online Fig. IG). However, we observed almost complete absence of 'whorl-shaped' lysosomes in these cells compared to control cells (Online Fig. IG, right panel), providing ultrastructural evidence of altered lysosomal lipid composition. To strengthen these observations, human THP-1 macrophages were co-cultured in vitro with BODIPY-prelabeled apoptotic Jurkat cells in the presence or absence of lalistat and confocal microscopy was performed to visualize the diffusion of cholesterol within intracellular compartments. LysoTracker staining (red) revealed that a considerable amount of BODIPY (green) was localized in the phagolysosomal membrane surrounding the apoptotic cells (yellow staining: overlap between green apoptotic cells and red LysoTracker staining) in lalistat-treated efferocytes (Online Fig. IH). In contrast, BODIPY (green) diffused within intracellular compartments in control and LIPA overexpressing THP-1 efferocytes (Online Fig. IH). Performing 3D reconstruction from confocal Z-stack images more clearly revealed the BODIPY lining surrounding apoptotic cells in lalistat-treated THP-1 efferocytes (Fig. 1H). Thus, LIPA is a key lysosomal enzyme that processes cholesteryl esters ingested from apoptotic cells during efferocytosis.

Defective lysosomal cholesterol hydrolysis does not initiate LC3-associated phagocytosis (LAP) or lysosomal dysfunction after efferocytosis.

During phagocytosis, LAP is a process by which LC3-II conjugation to phagosomes enables phagosome-lysosome fusion, stabilization of the NADPH oxidase 2 (NOX2) complex and apoptotic cell corpse clearance,[20] and we previously reported that NOX2 translocates to phagolysosomes in a cholesterol-dependent fashion.[21] Western blot analysis of LC3-II/LC3-I ratio showed that inhibition of LIPA in THP-1 macrophages did not alter LAP-engaged phagosome between 0 and 6 hours after efferocytosis (Fig. 2A and 2B). Although both LC3-I and LC3-II forms were reduced in LIPA overexpressing THP-1 macrophages, the LC3-II/LC3-I ratio was also not significantly modified between 0 and 6 hours after efferocytosis (Online Fig. IIA). We also investigated active NADPH oxidase (NOX) complex formation by immunostaining for p47^{phox} clustering, one of the active components of the NOX2 complex. As expected, a considerable amount of p47^{phox} staining (red) was localized to phagolysosomal membranes surrounding the apoptotic cells 1 hour post-efferocytosis; however, quantification of the phagolysosomal p47^{phox} staining did not reveal any difference between the control and lalistat-treated macrophages (Online Fig. IIB). Consistent with the role of the NOX complex in controlling phagolysosomal pH,[20] similar lysosomal acidification was observed between control and lalistat-treated efferocytes as measured by confocal microscopy 1 hour following the ingestion of apoptotic cells (Online Fig. IIC) or by flow cytometry using a LysoSensor probe (Online Fig. IID). LIPA overexpressing THP-1 macrophages also exhibited similar lysosomal acidification response

(Online Fig. IID). Altogether, our data indicate that defective lysosomal cholesterol hydrolysis does not initiate phagolysosome dysfunction after efferocytosis.

Defective autophagy or lysosomal biogenesis promotes macrophage apoptosis,[16,22,23] and we previously reported that defective efferocytosis could be the consequence of an excess cholesterol accumulation that induces apoptosis.[21] Western blot analysis revealed an increase in LC3II/LC3-I ratio 24 hours post-efferocytosis in lalistat-treated THP-1 macrophages, indicative of an enhanced autophagic response (Figs. 2A and 2B). We also observed an increased number of lysosomes in lalistat-treated THP-1 macrophages 24 hours post-efferocytosis using the LysoTracker probe and flow cytometry (Online Fig. IIE). The dephosphorylated form of TFEB is essential for optimal TFEB activation through translocation into the nucleus and subsequent activation of a gene network regulating lysosomal biogenesis and autophagy.[24] Inhibition of LIPA in macrophages led to an increase in the dephosphorylated form of TFEB 24 hours after ingestion of apoptotic cells (Figs. 2A and 2B), evoking an adaptive rather than a defective lysosomal biogenesis or autophagic response. Consistently, apoptosis was unaffected in LIPA deficient THP-1 efferocytes (LIPA knockdown using siRNA or lentiviral ShRNA particles) or lalistat-treated THP-1 efferocytes (Online Fig. IIF). In contrast, LIPA-overexpressing efferocytes exhibited lower autophagic and lysosomal biogenesis responses as shown by reduced expression of the dephosphorylated form of TFEB and both forms of LC3-I and LC3-II (Online Fig. IIA) and reduced LysoTracker staining (Online Fig. IIE). However, apoptosis was also unaffected in these cells (Online Fig. IF). Thus, lysosomal cholesterol hydrolysis capacity dictates TFEB-dependent lysosomal biogenesis and this adaptive compensatory response is unlikely the cause of defective efferocytosis but rather prevents macrophage from apoptosis.

Activation of the NLRP3 inflammasome causes defective efferocytosis after LIPA inhibition.

To evaluate whether LIPA-dependent lysosomal cholesterol storage ties lysosomal inflammation,[25] to defective efferocytosis, we next assessed the secretion of lysosomal inflammatory markers cathepsin B, K and IL-1β after ingestion of apoptotic cells. Consistent with the absence of lysosomal damage after LIPA inhibition, similar secretion of cathepsin B and K were observed between control and lalistat-treated THP-1 efferocytes (Figs. 2C and Online Fig. IIA). However, higher IL-1β and IL-18 secretion was observed 3h after LIPA inhibition in THP-1 efferocytes (Fig. 2D). Similar findings were observed after LIPA inhibition in murine thyoglycollate-elicited peritoneal efferocytes (Online Fig. IIIB). The NLRP3 inflammasome, which is a well-known sensor of danger signals, is involved in caspase-1-dependent maturation and secretion of IL-1β and IL-18.[26] Consistently, an inhibitor of NLRP3 (CP-456773) prevented the enhanced IL-1β and IL-18 secretion in lalistat-treated THP-1 efferocytes (Fig. 2D). Reduced IL-1β secretion, but not cathepsin B, was also observed in LIPA-overexpressing THP-1 efferocytes (Figs. 2C and Online Fig. IIIC). A time-course experiment confirmed an 100% increase in caspase-1 cleavage in THP-1 efferocytes as early as 3 hours after lalistat treatment, and this was sustained up to 24 hours following the ingestion of apoptotic Jurkat cells in lalistat-treated efferocytes (Figs. 2E). This result was associated with an increase in FAM-Flica caspase-1 activity that could be prevented by the NLRP3 inhibitor (Online Fig. IIID). Using immortalized murine NLRP3-deficient macrophages, we confirmed the dependence of the NLRP3 inflammasome on IL-1β secretion (Fig. S3E) and caspase-1 activation (Online Fig. IIIF) after LIPA inhibition. Inhibition of the NLRP3 inflammasome partially restored the efferocytic index of lalistat-treated THP-1 efferocytes (Fig. 2F). CP-456773 treatment and caspase 1 deficiency also prevented the efferocytosis defect induced by LIPA inhibition in murine thyoglycollate-elicited peritoneal efferocytes (Online Fig. IIIG). Thus, lysosomal cholesterol hydrolysis prevents the NLRP3 inflammasome-activating danger signal during efferocytosis to allow efficient clearance of apoptotic cells.

Caspase-1 activation has been previously proposed to cleave Rac1,[27] which is a canonical Rho guanosine triphosphatase (GTPase) involved in cytoskeletal reorganization and efferocytosis.[28] Transmission electron microscopy showed that the morphology of lalistat-treated THP-1 efferocytes

differed from control cells after 24 hours of culture with a less identifiable phagocytic cup that transform from filopodia and underlying lamellipodia (Online Fig. IIIH). Immunostaining for Rac1 (green) and F-actin (red) 6 hours after efferocytosis revealed a considerable amount of co-staining at the leading edge of membrane ruffle formation surrounding the apoptotic cells in control macrophages (overlapping yellow staining) (Online Fig. IIII, upper panels). In contrast, a general decrease in phagolysosome Rac1 was observed after LIPA inhibition (Online Fig. IIII, lower panels). This was more clearly visible after we performed 3D reconstruction from confocal Z-stack images (Fig. 2G). Reduced Rac1 protein expression was confirmed in THP-1 efferocytes after LIPA inhibition by Western blot (Fig. 2H). Pull-down activation assay confirmed reduced Rac1 activity after LIPA inhibition (Fig. 2H). To determine when after LIPA inhibition this decline in cell ruffling occurs, we used impedance to perform real-time monitoring of cell protrusion dynamics.[29] These analyses revealed increased resistance in lalistat-treated THP-1 macrophages beginning 6 hours post-efferocytosis (Fig. 2I), a signature that followed the inflammasome activation. We confirmed that the Rac1 inhibitor NSC23766, known to selectively lower active Rac1-GTP levels, also increased resistance in control cells to the level of lalistat-treated efferocytes (Fig. 2I). Inhibition of the NLRP3 inflammasome (CP-456773 treatment) rescued Rac1 protein expression (Fig. 2H). These findings provide a mechanism by which inflammasome-activating danger signal contributes to the defective efferocytic response after LIPA inhibition.

Defective lysosomal cholesterol hydrolysis repurposes MAM-dependent mitochondrial metabolism to activate the NLRP3 inflammasome and dampen efferocytosis.

Recent evidences suggest that LIPA is important for mitochondrial oxidative phosphorylation,[15] and elevated mitochondrial ROS production have been proposed to activate the NLRP3 inflammasome.[30] Reduced metabolic flux in the mitochondria of lalistat-treated THP-1 efferocytes was reflected by a decrease in the oxygen consumption rate (OCR) at baseline or after the inhibition of oxidative phosphorylation by oligomycin treatment (Figs. 3A and Online Fig. IVA). The enhanced OCR response was also prevented in thyoglycollate-elicited peritoneal efferocytes after LIPA inhibition or in LIPA deficient efferocytes (Online Fig. IVB). The increased capacity of LIPA-overexpressing THP-1 cells to capture and take up apoptotic Jurkat cells was also associated with increased oxygen consumption rate (OCR) and maximal respiration response after FCCP treatment (Fig. 3A). These observations were further supported by reduced mitochondrial uncoupling protein 2 (*ucp2*) mRNA expression in lalistat-treated THP-1 efferocytes (Online Fig. IVC) and enhanced mRNA levels of heme oxygenase-1 (*Hmox1*) (Fig. S4D) starting 1 hour after efferocytosis. Reduced mitochondrial flux and uncoupling of lalistat-treated THP-1 efferocytes paralleled an increase in mitochondrial ROS generation (Figs. 3B and 3C). This effect was most likely due to a raise in mitochondrial potential ($\Delta\Psi_m$) since addition of the complex I inhibitor (rotenone), the complex II inhibitor (3-nitropropionic acid, 3-NPA) or the succinate oxidation inhibitor (dimethyl malonate, DMM) promoted mitochondrial ROS production in control cells but not in lalistat-treated THP-1 efferocytes (Fig. 3C). These inhibitors also resulted in an increase in IL-1β secretion in control but not in lalistat-treated efferocytes (Fig. 3D).

Calcium is a central player in mitochondria metabolic repurposing and inflammasome activation,[31,32] and different lysosomal storage diseases have been associated with calcium flux modulation.[33-35] We first activated the two main lysosomal calcium pathways, the nicotinic acid adenine dinucleotide phosphate receptor (NAADPR) with the membrane-permeant NAADP analog (NAADP-AM) and the mucolipin transient receptor potential channel 1 (TRPML1) with the mucolipin synthetic agonist (ML-SA1). However, these treatments did not modify FAM-Flica caspase-1 activity or IL-1β secretion (Online Fig. IVE and IV4F). In contrast, activation of the mitochondrial inositol trisphosphate receptor (IP3R) with low dose 2-aminoethyl diphenylborinate (2-ABP) completely prevented the inflammasome activation and IL-1β secretion in lalistat-treated efferocytes (Online Figs. IVE and IVF). These findings suggest that inhibition of LIPA promotes mitochondrial metabolic repurposing-dependent inflammasome

activation by limiting mitochondrial calcium flux. To directly test this hypothesis, efferocytes were loaded with the calcium probe Fluo4-AM and calcium release from the mitochondria, a surrogate of mitochondrial calcium content, was assessed after treatment of cells with the mitochondrial uncoupler, carbonyl cyanide 3-chlorophenylhydrazone (CCCP). We observed a striking decrease in mitochondrial calcium release in lalistat-treated THP-1 efferocytes compared to control cells (Fig. 3E). Calcium-dependent activation of the inflammasome relies on Mitochondria-Associated ER Membranes (MAMs) that comprise IP3R and chaperone proteins.[32] Transmission electron microscopy highlighted ER-mitochondria contacts in control THP-1 efferocytes, an effect that was less visible in lalistat-treated cells (Fig. 3F). The ER-localized chaperone GRP78 (BiP) is part of the MAM macromolecular complex and interacts with ER lipid transporters.[37] Overexpression of GRP78 normalized the mitochondrial calcium response of lalistat-treated THP-1 efferocytes (Fig. 3E) and prevented the exacerbated IL-1β secretion (Fig. 3G). Consistently, GRP78 overexpression also restored efficient efferocytosis in lalistat-treated efferocytes (Fig. 3H). Thus, we propose that LIPA is required for MAM-dependent calcium flux after efferocytosis. This flux will repurpose the mitochondria to limit the inflammasome activating danger signal and allow efficient efferocytosis.

LIPA primes the sterol-dependent metabolic reprogramming of efferocytes.

The group of Cyster recently reported that defective 25-OH cholesterol generation in the ER promotes inflammasome activation in macrophages.[37,38] Thus, we next quantified sterol metabolites using liquid chromatography-mass spectrometry in control and lalistat-treated THP-1 macrophages 3 hours post-efferocytosis. Precursors of cholesterol synthesis such as lanosterol, 24-DH-lanosterol, 7-DH cholesterol and desmosterol as well as toxic sterols such as α-triols (cholesterol-3beta,5alpha,6beta-triol), α-Epox (cholesterol-5alpha,6alpha-epoxide), 7α-OH cholesterol and 7-ketocholesterol (7-KC) were not altered at this time point in lalistat-treated efferocytes (Online Fig. VA and VB). The brain-specific 24S-OH cholesterol was near the detection limit and was unaltered in lalistat-treated efferocytes (Fig. 4A). In contrast, a striking 50 to 70% decrease in oxysterols made from free cholesterol in the ER, such as 4β-OH cholesterol and 25-OH cholesterol or in the mitochondria such as 27-OH cholesterol, was observed in lalistat-treated efferocytes (Fig. 4A). These decreases were not associated with significant changes in the mRNA expression of the related oxysterol biosynthetic enzymes in lalistat-treated efferocytes (Online Fig. VC), suggesting that LIPA inhibition impacts the production of oxysterols by limiting substrate availability.

Part of the mechanism by which defective 25-OH cholesterol generation activates the inflammasome relies on modulation of cholesterol biosynthetic genes.[37,38] The ingestion of apoptotic cells led to a decrease in the mRNA expression of the biosynthetic genes *Srebf2* and *Hmgcr* in control macrophages starting 3 hours after efferocytosis, an effect that was virtually absent in lalistat-treated THP-1 macrophages (Figs. 4B, Online VD and VE). In contrast, *Srebf2* and *Hmgcr* mRNA expression were further intensified in LIPA-overexpressing THP-1 macrophages 3 hours after efferocytosis (Fig. 4B). Treatment of the cells with 25-OH cholesterol restored the down-regulation of *Srebf2* and *Hmgcr* mRNA expression in lalistat-treated efferocytes (Fig. 4B). These findings suggest that cholesteryl ester hydrolysis of engulfed apoptotic cells favors the flux of free cholesterol toward the ER (Online Fig. IE) to generate 25-OH cholesterol and dampen cholesterol biosynthetic pathway after efferocytosis. Treatment with 25-OH cholesterol partially restored the decrease in OCR observed in lalistat-treated THP-1 efferocytes (Fig. 4C) and rescued their mitochondrial calcium defect (Fig. 4D), offering a potential mechanism by which 25-OH cholesterol could control ER-dependent mitochondrial proticity after efferocytosis. Consistently, treatment with 25-OH cholesterol reduced inflammasome activation following efferocytosis in lalistat-treated THP-1 macrophages, as reflected by reduced IL-1β secretion (Fig. 4E) and restored an efficient efferocytic response (Fig. 4F). Treatment of Lipa deficient murine macrophages with 25-OH cholesterol also rescued the defective efferocytosis of these cells (Online Fig. VF). The reduced IL-1β secretion in LIPA-overexpressing efferocytes was also abolished after knockdown of Ch25h by siRNA (Online Fig. VG). Thus, we propose that impaired 25-OH cholesterol generation after LIPA inhibition controls

mitochondrial metabolic repurposing to activate the inflammasome and limit subsequent clearance of apoptotic cells.

25-OH and 27-OH cholesterol are potent endogenous LXR agonists and LXR activation occurs after efferocytosis to support efficient efferocytosis through upregulation of cholesterol efflux transporters or the efferocytic receptor *MertK*.[21,39] Thus, we next examined the expression of LXR target genes during the course of efferocytosis and observed that the mRNA expression of the cholesterol efflux transporters *Abca1* and *Abcg1* was not altered in the early phase of efferocytosis in lalistat-treated THP-1 macrophages (up to 6 hours) but was significantly decreased in the late resolution phase (Online Fig. VIA and VIB). Cholesterol efflux studies have confirmed a decrease in cholesterol efflux to lipid-poor apoA-1, the major apolipoprotein of HDL (Online Fig. VIC) and to PEG-HDL (Online Fig. VID) 24 hours after the ingestion of apoptotic cells in lalistat-treated THP-1 macrophages. In contrast, LIPA-overexpressing THP-1 efferocytes exhibited higher mRNA expression of LXR target genes (Online Fig. VIE) and more cholesterol efflux to PEG HDL (Online Fig. VIF). We confirmed the LXR dependency of these effects, as treatment with the synthetic LXR agonist TO901317 not only enhanced the expression of *Abca1* and *Abcg1* (Online Fig. VIG) but also cholesterol efflux to HDL in lalistat-treated THP-1 macrophages (Online Fig. VIH). Consistently, we observed reduced mRNA expression of the efferocytic receptor *MertK* in lalistat-treated THP-1 macrophages 24 hours after efferocytosis (Fig. 4G). In contrast, *MertK* was upregulated in LIPA-overexpressing THP-1 efferocytes (Online Fig. VIE). To delineate whether LXR activation could rescue the adverse effects of LIPA inhibition on efferocytes, stimulation of LXR activity was achieved with 25-OH cholesterol, 27-OH cholesterol or the synthetic LXR agonist TO901317 for 24 hours. In contrast to 25-OH cholesterol treatment, 27-OH cholesterol or TO901317 did not prevent the inflammasome activation (Fig. 4E). However, all treatments enhanced *MertK* mRNA expression in control and lalistat-treated THP-1 efferocytes (Fig. 4G). This could explain how 27-OH cholesterol and TO901317 partially restored the efferocytic capacity of lalistat-treated efferocytes (Fig. 4F). The relevance of this pathway was further illustrated through the effect of the LXR agonist in synergizing with the NLRP3 inhibitor (CP-456773) to fully restore efficient efferocytosis (Fig. 4H). These results indicate that LXR activation is a critical checkpoint by which LIPA controls the efferocytic response.

Altogether, these findings reveal that LIPA favors efficient efferocytosis through sterol-dependent metabolic reprogramming: 1) The ER-dependent 25-OHC generation after lysosomal cholesterol hydrolysis will limit inflammasome activating danger signal and prevent Rac1-dependent phagocytic cup disassembly and 2) 25- and 27-OHC generation after lysosomal cholesterol hydrolysis will activate a LXR-dependent transcriptional program that favors ABCA1 and ABCG1-dependent efflux of cholesterol ingested from apoptotic cells and primes efferocytes for multiple MertK-dependent clearance of apoptotic cells.

LIPA orchestrates disposal of stressed erythrocytes and apoptotic cells in vivo.

Taking advantage of a publicly available gene expression dataset from Immgen (http://immgen.org), we observed that efferocytosis markers, LXR target genes and heme and iron homeostasis markers were predominantly expressed not only in peritoneal macrophages but also in specialized tissue-resident macrophages, paralleling LIPA expression and lysosome markers (Online Fig. VIIA). This finding suggested an important interplay between LIPA, cholesterol homeostasis and tissue-resident macrophage lysosomal and erythrophagocytic functions. The in vivo contribution of LIPA to efferocytosis was next studied using two different models. The use of lalistat treatment over LIPA deficient mice was chosen to avoid an inflammatory phenotype that could origin from embryogenesis.[12] We intravenously injected either fluorescently labeled stressed erythrocytes (sRBCs) or apoptotic lymphocytes (ALs) into mice treated with lalistat or vehicle for 2 weeks and examined their macrophage efferocytic capacity in spleen and liver 16 hours later. sRBCs and ALs were retrieved in the liver and spleen (Online Fig. VIIB) and accumulated within different leukocyte populations gated by flow cytometry as $CD11b^{lo}F4/80^{int}$ myeloid cells, $CD11b^{lo}F4/80^{high}$ Kupffer cells (KCs) or red pulp macrophages (RPMs) and $CD11b^{high}F4/80^{high}$ whether

these cells are the newly identified transient macrophage population (T-macs) or a subpopulation of myeloid cells (Fig. 5A).[40] In the liver, sRBCs and to a lesser extent ALs promoted the appearance of T-macs or a subpopulation of myeloid cells (Fig. 5A). Both T-macs and KCs ingested labeled sRBCs or ALs (Figs. 5B and Online Fig VIIC). A small fraction of myeloid cells also ingested fluorescent sRBCs or ALs (Fig. 5B and Online Fig. VIIC). Lalistat treatment reduced the ability of KCs and T-macs to phagocytose labeled sRBCs and ALs (Fig. 5B and Online Fig VIIC). However, lalistat also induced a compensatory increase in the number of myeloid cells that had phagocytosed labeled ALs (Online Fig. VIIC). In the spleen, RPMs were the most abundant cell population that efficiently cleared labeled sRBCs and ALs (Fig. 5C and Online Fig VIID). Lalistat treatment reduced the efferocytic capacity of RPMs (Fig. 5C and Online Fig VIID) and there was a specific compensatory up-regulation of the number of myeloid cells that had ingested ALs (Online Fig. VIID). The enhanced number of immature myeloid cell with efferocytic capacity after lalistat treatment was a specific response to the injection of ALs, most likely reflecting the initiation of an inflammatory response secondary to release of find-me or danger signals in this context.[29] We thus conclude that LIPA promotes the disposal of stressed RBCs and apoptotic cells in hepatic and splenic macrophage populations.

LIPA inhibition precipitates hypercholesterolemia-associated efferocytosis defects.

Previous studies have documented defective efferocytosis and splenomegaly under hypercholesterolemic conditions.[2] Thus, high-fat diet-fed hypercholesterolemic *Ldlr*$^{-/-}$ mice were next treated with lalistat for 2 weeks. An analysis of macrophage numbers in the spleen (RPMs), liver (KCs), adipose tissue (ATMs) and peritoneal cavity (PMs) (Online Fig. VIIIA) revealed a specific increase in RPMs and KCs, probably to compensate for efferocytosis defects, but not in ATMs or PMs (Online Fig. VIIIB). Consistent with this observation, reduced mRNA expression of efferocytic markers (i.e, MertK, Axl and Gas6) were down regulated by lalistat treatment along with enhanced inflammatory markers including Il1β (Fig. 5D). RPMs from lalistat-treated animals also exhibited reduced cell surface expression of CD206 (the mannose receptor MRC1) (Online Fig. VIIIC). Mechanistically and in line with our in vitro studies, LIPA inhibition led to a compensatory increase in lysosomal biogenesis in RPMs and KCs with no changes in lysosomal acidification as quantified by flow cytometry (Online Fig. VIIID). This result correlated with enlarged spleen and higher splenic IL-1β levels in lalistat-treated animals while other inflammatory parameters were unaffected (Table 1). Senescent RBCs are normally phagocytosed by macrophages in the spleen and liver, and defective erythrophagocytosis leads to splenic iron deposition.[41,42] Thus, we assessed iron stores in lalistat-treated animals. Splenic iron accumulation was histologically evident and was largely confined to the red pulp in lalistat-treated animals (Fig. 5E). Plasma, liver, and adipose tissue iron and ferritin concentrations were normal in lalistat-treated animals (Fig. 5F-5G and Table 1), but an increased iron concentration was confirmed in the spleen (Fig. 5F). Ferritin concentrations were also increased by more than 200% in the spleens of lalistat-treated animals but did not reach statistical significance (P=0.07, Fig. 5G). Thus, our data supports a critical in vivo role of LIPA in the efferocytic capacity of tissue-resident macrophages under hypercholesterolemic conditions, which is required for tissue integrity by maintaining immune and tissue lipid homeostasis.

DISCUSSION

Macrophage lipid accumulation and defective clearance of apoptotic cells are central events in many metabolic disorders. However, the specific molecular mechanisms linking lipid accumulation to inflammation in macrophages are still not completely understood. We have now uncovered a novel mechanism by which LIPA controls macrophage inflammatory response by limiting continued clearance of apoptotic cells. Notably, our mechanistic studies demonstrated that lysosomal cholesterol hydrolysis mediated by LIPA orchestrated the timely production of 25-OH and 27-OH cholesterol during efferocytosis, which modulated inflammasome activation and the generation of endogenous LXR ligands. While activation of the inflammasome after LIPA inhibition led to defects in Rac1-dependent phagocytic cup formation, decreased production of LXR ligands resulted in reduced cholesterol efflux and *MertK* expression impeding subsequent apoptotic cell clearance (Graphical abstract, Fig. 6). Importantly, our findings indicate that in vivo inhibition of this pathway reduced the clearance of apoptotic lymphocytes and stressed erythrocytes by splenic- and hepatic-resident macrophages leading to splenomegaly and splenic iron accumulation upon hypercholesterolemic challenge. Collectively, these findings demonstrate the importance of macrophage lysosomal cholesterol hydrolysis linking metabolism and inflammation under homeostatic and disease conditions.

It has been shown that LIPA is essential for breaking down fatty material within the lysosomal compartment of macrophages upon receptor-mediated endocytosis of lipoprotein, lysosome biogenesis or lipophagy,[14,15,22] but the relevance to efferocytosis has not yet been addressed. Our findings reveal that LIPA activity follows the efferocytic capacity of polarized macrophages and controls the lysosomal degradative capacity under non-polarizing culture conditions raising a number of interesting questions for future study. First, the dual role of LIPA for optimal alternative macrophage activation,[14] and efferocytosis, as detailed in the present study, might be interconnected in vivo to promote tissue repair and metabolic homeostasis.[43] The findings of reduced LIPA activity in classically activated macrophages and enhanced inflammasome activation after LIPA inhibition also indicates that LIPA might be more susceptible to exogenous inflammatory stimuli. Thus, it will be of interest to determine whether LIPA may prime macrophages prior activation. Indeed, a switch between classically and alternatively activated macrophages was previously associated to different oxidative stress responses that prime macrophage prior activation.[44,45]

Second, why enhanced oxidative stress does not initiate apoptosis after LIPA inhibition needs to be defined. While our data exclude a role of NADPH oxidase in promoting cholesterol-dependent apoptosis susceptibility,[21] they do not rule out why mitochondrial oxidative stress and associated inflammasome activation are not linked to pyroptosis or other forms of apoptosis. One explanation could be the absence of second signals that triggers apoptosis ('two hit models'),[8] or the level of aggressiveness of the first signal. For instance, we found occasional cholesterol crystals in macrophages after LIPA inhibition and no sign of lysosomal damage after apoptotic cell clearance despite higher NLRP3 inflammasome activation. These findings contrast with the activation of the NLRP3 inflammasome by cholesterol crystals relying on lysosomal damage and the subsequent proteolytic activation of cathepsins.[9,17] This could be the consequence of an accumulation of cholesteryl ester after LIPA inhibition rather than free cholesterol, which is the source of cholesterol crystal formation in lysosomes.[46] Another possibility for the lack of apoptosis induction after LIPA inhibition could involve formation of new lysosomes to face cholesterol accumulation that has been previously shown to prevent cell death.[23] It also remains an open question as to how exactly the origin and level of mitochondrial ROS, which depends on the balance between the reverse electron transport of the electron transport chain and the mitochondrial potential ($\Delta\Psi_m$),[47] leads to oxidative damage to DNA, proteins and lipids and subsequent apoptosis. It would be of interest to determine whether absence of ROS-mediated mtDNA release after LIPA inhibition may have limited activation of the AIM2 inflammasome under efferocytic condition since AIM2 has redundant function with the NLRP3 inflammasome,[38] and activates apoptosis.

How does LIPA control optimal clearance of apoptotic cells? Our findings suggest that inhibition of lysosomal cholesteryl ester hydrolysis limited the generation of free cholesterol that could reach sites of oxysterol generation after the digestion of apoptotic cells. These oxysterols include 25-OH and 27-OH cholesterol that could prime efferocytes for subsequent apoptotic cell clearance by at least two independent mechanisms. We first observed an unexpected mechanism that involves defective production of 25-OH cholesterol in the ER, which impaired the repression of cholesterol biosynthetic genes post-efferocytosis but also prevented MAM-dependent mitochondrial metabolic repurposing and subsequent activation of the inflammasome. This activation reduced Rac1 activity and subsequently disorganized phagocytic cups. Although it was recently shown that defective 25-OH cholesterol generation in macrophages promotes inflammasome activation,[37,38] the present study positions this observation in the context of efferocytosis and provides new insights into the underlying mechanisms. Indeed, we found that 1) LIPA controls the generation of 25-OH cholesterol after efferocytosis and 2) 25-OH cholesterol controls the MAM-dependent calcium flux to repurpose mitochondrial metabolism. Under normal physiological conditions, calcium primarily promotes ATP synthesis by stimulating enzymes of the Krebs cycle and oxidative phosphorylation in the mitochondria. This increased metabolic rate would consume more oxygen resulting in increased respiratory chain electron leakage and mitochondrial ROS levels as it is observed in control efferocytes. After LIPA inhibition, reduced mitochondrial calcium influx may have dampened OXPHOS and UCP-2-dependent proton leaks across the inner mitochondrial membrane but at the same time reduced $\Delta\Psi_m$ consumption exacerbating mitochondrial ROS generation.[30,31] Restoring MAM-dependent calcium flux through GPR78 overexpression was sufficient to prevent the inflammasome activation after LIPA inhibition mimicking the effect of 25-OH cholesterol. Future studies will be required to understand whether MAM formation during efferocytosis is also linked to mitochondrial fission.[48] Nevertheless, this mitochondrial checkpoint is crucial for the efferocytic response of macrophages as the inflammasome activation after LIPA inhibition reduced Rac1 expression and activity. Decreased levels of Rac1 and F-actin polymerization in membrane ruffles following the ingestion of apoptotic cells caused cytoskeletal changes and impaired pseudopod formation. Similar modulation of focal adhesion dynamics was previously observed under cholesterol loading conditions in LIPA deficient cells.[49] In our setting, this modulation contributed to reduce efferocytic capacity after LIPA inhibition.

Consistent with 25-OH and 27-OH cholesterol being potent LXR agonists in macrophages,[7,10] we next observed a delayed response in LXR target gene activation after LIPA inhibition in efferocytes leading to impaired cholesterol efflux and reduced efferocytic capacity.[21,39] We confirmed that reduced LXR activation was independent of, and synergized with, the modulation of Rac1 signaling pathway to impede efficient apoptotic cell clearance.[50] Interestingly, in other lysosomal storage diseases such as Niemann-Pick type C (NPC) disease, in which cholesterol accumulates within late endosomes, it has been reported that NPC cells exhibit a defect in 25-OH and 27-OH cholesterol in response to LDL and fail to repress SREBPs and LXRs.[51,52] Our findings extend these observations, and we propose that LIPA-dependent cholesteryl ester hydrolysis, which is upstream of endosomal NPC-dependent cholesterol trafficking, might be an earlier enzymatic step that governs oxysterol generation and LXR activation during efferocytosis. Thus, LIPA-dependent lysosomal cholesterol hydrolysis orchestrates the timely cholesterol-dependent inflammasome activation and transcriptional efferocytic response of macrophages.

On a daily basis, over 100 billion white and red blood cells are turned over through efferocytosis to prevent the inflammatory consequences associated with the accumulation of apoptotic debris and to maintain tissue homeostasis.[8,28] Although the splenomegaly of LIPA-deficient mice has been associated with extramedullary hematopoiesis,[12] the spleen does not support hematopoiesis in humans under injury-free conditions,[53] arguing that defective efferocytosis is most likely the culprit of the inflammatory phenotype and splenomegaly of LIPA mutation carriers.[11] Considerable data support that dying cells are normally phagocytosed by macrophages in the spleen and liver, and apoptotic bodies are rapidly broken down into their molecular constituents, including iron and lipids, which must be recycled or transported back into the circulation.[41,42] Challenging mice with stressed RBCs or apoptotic lymphocytes revealed that LIPA

inhibition attenuated the efferocytic capacity of not only red pulp macrophages but also Kupffer cells. Under hypercholesterolemic disease conditions, we found that LIPA inhibition caused the spontaneous accumulation of iron in the spleen along with enhanced splenic IL-1β content. These findings could have major relevance not only for current enzyme replacement therapy for LIPA mutation carriers but also to better elucidate the recent genome-wide association studies (GWAS) that have reinforced LIPA as a susceptibility gene for cardiovascular diseases along with reduced LIPA activity.[54,55]

ACKNOWLEDGMENTS

We thank Dr. Wanida Ruangsiriluk for providing LIPA overexpressing THP-1 macrophages and very useful scientific discussion and advice. We thank Dr. Fréderic Larbret for assistance with flow cytometry and Dr. Véronique Corcelle for assistance in animal facilities.

SOURCES OF FUNDING

The Fondation ARC (RAC15014AAA) and the Austrian Science Fund (W1226 DK-MCD) support L.B and D.K, respectively. PACA region PhD fellowship supports M.V and BioTechMed-Graz (Flagship) supports N.V and M.D.M fellowships. This work was supported by the Inserm Atip-Avenir program, the association VML (Vaincre les Maladies Lysosomales), the European Marie Curie Career Integation Grant (CIG-630926) and the Agence Nationale de la Recherche (ANR-14-CE12-0017-01) to L.Y.C.

DISCLOSURES

None**.**

REFERENCES

1. Wynn, T.A., Chawla, A., and Pollard, J.W. (2013). Macrophage biology in development, homeostasis and disease. Nature *496*, 445–455.
2. Tall, A.R., and Yvan-Charvet, L. (2015). Cholesterol, inflammation and innate immunity. Nat. Rev. Immunol. *15*, 104–116.
3. Han, C.Z., and Ravichandran, K.S. (2011). Metabolic connections during apoptotic cell engulfment. Cell *147*, 1442–1445.
4. Nagata, S., Hanayama, R., and Kawane, K. (2010). Autoimmunity and the clearance of dead cells. Cell *140*, 619–630.
5. Maxfield, F.R., Tabas, I. Role of cholesterol and lipid organization in disease. (2005). Nature. *438*, 612-21.
6. Goldstein, J.L., DeBose-Boyd, R.A., and Brown, M.S. (2006). Protein sensors for membrane sterols. Cell *124*, 35–46.
7. Spann, N.J., and Glass, C.K. (2013). Sterols and oxysterols in immune cell function. Nat. Immunol. *14*, 893–900.
8. Tabas, I. (2010). Macrophage death and defective inflammation resolution in atherosclerosis. Nat. Rev. Immunol. *10*, 36–46.
9. Duewell, P., Kono, H., Rayner, K.J., Sirois, C.M., Vladimer, G., Bauernfeind, F.G., Abela, G.S., Franchi, L., Nuñez, G., Schnurr, M., et al. (2010). NLRP3 inflammasomes are required for atherogenesis and activated by cholesterol crystals. Nature *464*, 1357–1361.
10. Zelcer, N., and Tontonoz, P. (2006). Liver X receptors as integrators of metabolic and inflammatory signaling. J. Clin. Invest. *116*, 607–614.
11. Bernstein, D.L., Hülkova, H., Bialer, M.G., and Desnick, R.J. (2013). Cholesteryl ester storage disease: review of the findings in 135 reported patients with an underdiagnosed disease. J. Hepatol. *58*, 1230–1243.

12. Du, H., and Grabowski, G.A. (2004). Lysosomal acid lipase and atherosclerosis. Curr. Opin. Lipidol. *15*, 539–544.
13. Yan, C., Lian, X., Li, Y., Dai, Y., White, A., Qin, Y., Li, H., Hume, D.A., and Du, H. (2006). Macrophage-specific expression of human lysosomal acid lipase corrects inflammation and pathogenic phenotypes in lal-/- mice. Am. J. Pathol. *169*, 916–926.
14. Huang, S.C.-C., Everts, B., Ivanova, Y., O'Sullivan, D., Nascimento, M., Smith, A.M., Beatty, W., Love-Gregory, L., Lam, W.Y., O'Neill, C.M., et al. (2014). Cell-intrinsic lysosomal lipolysis is essential for alternative activation of macrophages. Nat. Immunol. *15*, 846–855.

15. Ouimet, M., Franklin, V., Mak, E., Liao, X., Tabas, I., and Marcel, Y.L. (2011). Autophagy regulates cholesterol efflux from macrophage foam cells via lysosomal acid lipase. Cell Metab. *13*, 655–667.
16. Razani, B., Feng, C., Coleman, T., Emanuel, R., Wen, H., Hwang, S., Ting, J.P., Virgin, H.W., Kastan, M.B., and Semenkovich, C.F. (2012). Autophagy links inflammasomes to atherosclerotic progression. Cell Metab. *15*, 534–544.
17. Sheedy, F.J., Grebe, A., Rayner, K.J., Kalantari, P., Ramkhelawon, B., Carpenter, S.B., Becker, C.E., Ediriweera, H.N., Mullick, A.E., Golenbock, D.T., et al. (2013). CD36 coordinates NLRP3 inflammasome activation by facilitating intracellular nucleation of soluble ligands into particulate ligands in sterile inflammation. Nat. Immunol. *14*, 812–820.
18. Stitziel, N.O., Fouchier, S.W., Sjouke, B., Peloso, G.M., Moscoso, A.M., Auer, P.L., Goel, A., Gigante, B., Barnes, T.A., Melander, O., et al. (2013). Exome sequencing and directed clinical phenotyping diagnose cholesterol ester storage disease presenting as autosomal recessive hypercholesterolemia. Arterioscler. Thromb. Vasc. Biol. *33*, 2909–2914.
19. Bochem, A.E., van der Valk, F.M., Tolani, S., Stroes, E.S., Westerterp, M., and Tall, A.R. (2015). Increased Systemic and Plaque Inflammation in ABCA1 Mutation Carriers With Attenuation by Statins. Arterioscler. Thromb. Vasc. Biol. *35*, 1663–1669.
20. Green, D.R., Oguin, T.H., Martinez, J. (2016). The clearance of dying cells: table for two. Cell Death & Differentiation. *23*, 915-926.
21. Yvan-Charvet, L., Pagler, T.A., Seimon, T.A., Thorp, E., Welch, C.L., Witztum, J.L., Tabas, I., and Tall, A.R. (2010). ABCA1 and ABCG1 protect against oxidative stress-induced macrophage apoptosis during efferocytosis. Circ. Res. *106*, 1861–1869.
22. Emanuel, R., Sergin, I., Bhattacharya, S., Turner, J.N., Epelman, S., Settembre, C., Diwan, A., Ballabio, A., and Razani, B. (2014). Induction of lysosomal biogenesis in atherosclerotic macrophages can rescue lipid-induced lysosomal dysfunction and downstream sequelae. Arterioscler. Thromb. Vasc. Biol. *34*, 1942–1952.
23. Sergin, I., Evans, T.D., Zhang, X., Battacharya, S., Stokes, C.J., Song, E., Dehestani, B., Holloway, K.B., Micevych, P.S., Javaheri, A., Crowley, J.R., Ballabio, A., Schilling, J.D., Epelman, S., Weihl, C.C., Diwan, A., Fan, D., Zayed, M.A., Razani, B. (2017). Exploiting macrophage autophagy-lysosomal biogenesis as a therapy for atherosclerosis. Nat Commun. *8*,15750.
24. Settembre, C., Di Malta, C., Polito, V.A., Garcia Arencibia, M., Vetrini, F., Erdin, S., Erdin, S.U., Huynh, T., Medina, D., Colella, P., et al. (2011). TFEB links autophagy to lysosomal biogenesis. Science *332*, 1429–1433.
25. Weissmann, G. (1967). The role of lysosomes in inflammation and disease. Annu. Rev. Med. *18*, 97–112.
26. Lamkanfi, M., and Dixit, V.M,. (2017). In retrospect: The inflammasome turns 15. Nature. *548*, 534-535.
27. Sokolovska, A., Becker, C.E., Ip, W.K., Rathinam, V.A., Brudner, M., Paquette, N., Tanne, A., Vanaja, S.K., Moore, K.J., Fitzgerald, K.A., Lacy-Hulbert, A., Stuart, L.M. (2013). Activation of caspase-1 by the NLRP3 inflammasome regulates the NADPH oxidase NOX2 to control phagosome function. Nat. Immunol. *14*, 543-53.
28. Elliott, M.R., and Ravichandran, K.S. (2016). The Dynamics of Apoptotic Cell Clearance. Dev. Cell *38*, 147–160.

29. Giaever, I., and Keese, C.R. (1993). A morphological biosensor for mammalian cells. Nature. *366*, 591-592.
30. Zhou, R., Yazdi, A.S., Menu, P., Tschopp, J. (2011). A role for mitochondria in NLRP3 inflammasome activation. Nature. *469*, 221-226.
31. Brookes, P.S., Yoon, Y., Robotham, J.L., Anders, M.W., Sheu, S.S. (2004). Calcium, ATP, and ROS: a mitochondrial love-hate triangle. Am. J. Physiol. Cell. Physiol. *287*, C817-C833.
32. Horng, T. (2014). Calcium signaling and mitochondrial destabilization in the triggering of the NLRP3 inflammasome. Trends Immunol. *35*, 253-261.
33. Lloyd-Evans, E., Morgan, A., He, X., Smith, D.A., Elliot-Smith, E., Sillence, D.J., Churchill, G.C., Schuchman, E.H., Galione, A., Platt, F.M. (2008). Niemann-Pick disease type C1 is a sphingosine storage disease that causes deregulation of lysosomal calcium. Nat Med. *14*, 1247-55.
34. Sano, R., Annunziata, I., Patterson, A., Moshiach, S., Gomero, E., Opferman, J., Forte, M., d'Azzo, A. (2008). GM1-Ganglioside accumulation at the Mitochondria-Associated ER membranes links ER stress to Ca^{2+}-dependent mitochondrial apoptosis. Molecular Cell. *36*, 500-511.
35. Shen, D., Wang, X., Li, X., Zhang, X., Yao, Z., Dibble, S., Dong, X.P., Yu, T., Lieberman, A.P., Showalter, H.D., Xu, H. (2012). Lipid storage disorders block lysosomal trafficking by inhibiting a TRP channel and lysosomal calcium release. Nat Commun. *3*, 731.
36. Prasad, M., Pawlak, K.J., Burak, W.E., Perry, E.E., Marshall, B., Whittal, R.M., Bose, H.S. (2017). Mitochondrial metabolic regulation by GRP78. Sci Adv. *3*,e1602038.
37. Reboldi, A., Dang, E.V., McDonald, J.G., Liang, G., Russell, D.W., and Cyster, J.G. (2014). Inflammation. 25-Hydroxycholesterol suppresses interleukin-1-driven inflammation downstream of type I interferon. Science *345*, 679–684.
38. Dang, E.V., McDonald, J.G., Russell, D.W., Cyster, J.G. (2017). Oxysterol restraint of cholesterol synthesis prevents AIM2 inflammasome activation. Cell. *171*, 1-15.
39. A-Gonzalez, N., Bensinger, S.J., Hong, C., Beceiro, S., Bradley, M.N., Zelcer, N., Deniz, J., Ramirez, C., Díaz, M., Gallardo, G., et al. (2009). Apoptotic cells promote their own clearance and immune tolerance through activation of the nuclear receptor LXR. Immunity *31*, 245–258.
40. Theurl, I., Hilgendorf, I., Nairz, M., Tymoszuk, P., Haschka, D., Asshoff, M., He, S., Gerhardt, L.M.S., Holderried, T.A.W., Seifert, M., et al. (2016). On-demand erythrocyte disposal and iron recycling requires transient macrophages in the liver. Nat. Med. *22*, 945–951.
41. De Domenico, I., McVey Ward, D., and Kaplan, J. (2008). Regulation of iron acquisition and storage: consequences for iron-linked disorders. Nat. Rev. Mol. Cell Biol. *9*, 72–81.
42. Kohyama, M., Ise, W., Edelson, B.T., Wilker, P.R., Hildner, K., Mejia, C., Frazier, W.A., Murphy, T.L., and Murphy, K.M. (2009). Role for Spi-C in the development of red pulp macrophages and splenic iron homeostasis. Nature *457*, 318–321.
43. Wynn, T.A., Chawla, A., and Pollard, J.W. (2013). Macrophage biology in development, homeostasis and disease. Nature *496*, 445–455.
44. Jais, A., Einwallner, E., Sharif, O., Gossens, K., Lu, T.T.-H., Soyal, S.M., Medgyesi, D., Neureiter, D., Paier-Pourani, J., Dalgaard, K., et al. (2014). Heme oxygenase-1 drives metaflammation and insulin resistance in mouse and man. Cell *158*, 25–40.
45. Sarrazy, V., Sore, S., Viaud, M., Rignol, G., Westerterp, M., Ceppo, F., Tanti, J.-F., Guinamard, R., Gautier, E.L., and Yvan-Charvet, L. (2015). Maintenance of Macrophage Redox Status by ChREBP Limits Inflammation and Apoptosis and Protects against Advanced Atherosclerotic Lesion Formation. Cell Rep *13*, 132–144.
46. Kellner-Weibel, G., Yancey, P.G., Jerome, W.G., Walser, T., Mason, R.P., Phillips, M.C., and Rothblat, G.H. (1999). Crystallization of free cholesterol in model macrophage foam cells. Arterioscler. Thromb. Vasc. Biol. *19*, 1891–1898.
47. Scialò, F., Fernandez-Ayala, D.J., Sanz, A. (2017). Role of mitochondrial reverse electron transport in ROS signaling: potential roles in health and disease. Front Physiol. *8*,428.

48. Wang, Y., Subramanian, M., Yirdagul, A., Barbosa-Lorenzi, V.C., Cai, B., de Juan-Sanz, J., Ryan, T.A., Nomura, M., Maxfield, F.R., Tabas, I. (2017). Mitochondrial fission promotes the continued clearance of apoptotic cells by macrophages. Cell. *171*, 1-15.
49. Kanerva, K., Uronen, R.-L., Blom, T., Li, S., Bittman, R., Lappalainen, P., Peränen, J., Raposo, G., and Ikonen, E. (2013). LDL cholesterol recycles to the plasma membrane via a Rab8a-Myosin5b-actin-dependent membrane transport route. Dev. Cell *27*, 249–262.
50. Fond, A.M., Lee, C.S., Schulman, I.G., Kiss, R.S., and Ravichandran, K.S. (2015). Apoptotic cells trigger a membrane-initiated pathway to increase ABCA1. J. Clin. Invest. *125*, 2748–2758.
51. Frolov, A., Zielinski, S.E., Crowley, J.R., Dudley-Rucker, N., Schaffer, J.E., and Ory, D.S. (2003). NPC1 and NPC2 regulate cellular cholesterol homeostasis through generation of low density lipoprotein cholesterol-derived oxysterols. J. Biol. Chem. *278*, 25517–25525.
52. Zhang, J.R., Coleman, T., Langmade, S.J., Scherrer, D.E., Lane, L., Lanier, M.H., Feng, C., Sands, M.S., Schaffer, J.E., Semenkovich, C.F., et al. (2008). Niemann-Pick C1 protects against atherosclerosis in mice via regulation of macrophage intracellular cholesterol trafficking. J. Clin. Invest. *118*, 2281–2290.
53. Crosby, W.H. (1983). Hematopoiesis in the human spleen. Arch. Intern. Med. *143*, 1321–1322.
54. Wild, P.S., Zeller, T., Schillert, A., Szymczak, S., Sinning, C.R., Deiseroth, A., Schnabel, R.B., Lubos, E., Keller, T., Eleftheriadis, M.S., et al. (2011). A genome-wide association study identifies LIPA as a susceptibility gene for coronary artery disease. Circ Cardiovasc Genet *4*, 403–412.
55. Morris, G.E., Braund, P.S., Moore, J.S., Samani, N.J., Codd, V., and Webb, T.R. (2017). Coronary Artery Disease-Associated LIPA Coding Variant rs1051338 Reduces Lysosomal Acid Lipase Levels and Activity in Lysosomes. Arterioscler. Thromb. Vasc. Biol. *37*, 1050-57.

FIGURE LEGENDS

Figure 1. LIPA expression controls efferocytic capacity and lysosomal cholesterol trafficking. (A) Correlations between LIPA activity and the efferocytic index in human THP-1 macrophages exposed for 16 hours to medium alone (M0), 50 ng/mL LPS (M1) or 15 ng/mL IL-4 (M2). (B) THP-1 macrophages were transduced with empty or LIPA ShRNA lentiviral particles or transfected with scrambled or LIPA SiRNA before incubation with Cell-Tracker Deep Red-prelabeled apoptotic Jurkat cells and quantification of the efferocytic index by flow cytometry. LIPA overexpressing cells (Ovex) were also used in this assay. (C) BODIPY staining was quantified by flow cytometry in THP-1 macrophages after modulation of LIPA expression (as described above) and exposure for 30 minutes to apoptotic Jurkat cells. Data are expressed as the mean fluorescence intensity (MFI). The dotted line represents the BODIPY-neutral lipid content into non-efferocytic control cells. (D-E) THP-1 macrophages (CD64+) were incubated for the indicated times in the presence or absence of 10 μM lalistat together with Cell-Tracker Deep Red-prelabeled apoptotic Jurkat cells, and the efferocytic index was quantified by flow cytometry. (F) THP-1 macrophages incubated in the presence or absence of 10 μM lalistat were stimulated with apoptotic Jurkat cells for the indicated times. BODIPY staining was quantified by flow cytometry. Inset depicts a representative histogram at the indicated time point. (G) Control or lalistat-treated THP-1 efferocytes, cultured for 1 hour after the ingestion of [^{3}H]-cholesterol-prelabeled apoptotic Jurkat cells, were fractionated by sucrose step gradient, and fractions were assayed for [^{3}H]-cholesterol incorporation as described in the Methods section. (H) Representative 3D reconstruction from confocal Z-stack images of an ingested apoptotic cell prelabeled with BODIPY (green) and localized within a phagolysosome (stained with LysoTracker^R Deep Red). Cells were counterstained with DAPI (nuclear staining). Arrows indicate BODIPY clusters in phagocytic cells (eight to ten different confocal images were analyzed per condition from experiments performed in triplicate). The data are given as the mean ± SEM of at least two experiments performed in triplicate. **P*<0.05 *vs.* controls.

Figure 2. Defective lysosomal cholesterol hydrolysis promotes lysosomal damage-independent inflammasome activation after efferocytosis causing subsequent Rac1-dependent phagocytic cup defects. (A) Representative immunoblots of LC3I/II and phospho-Tfeb from control or lalistat-treated THP-1 macrophages incubated for 30 minutes with apoptotic Jurkat cells and cultured for various times. (B) Kinetics of band densities normalized to HSP90 are shown for the indicated times. (C) Cathepsin B secretion levels from control or lalistat-treated THP-1 efferocytes cultured for the indicated times after the ingestion of apoptotic cells and expressed in ng/mL. (D) IL-1β and IL-18 secretion levels (expressed in pg/mL) from control or lalistat-treated THP-1 efferocytes cultured for 3 hours after the ingestion of apoptotic cells in the presence or absence of 25 nM Nlrp3 inflammasome inhibitor (CP456773). The dotted lines represent IL-1□ and IL-18 secretion levels into non-efferocytic control cells. (E) Immunoblot of caspase-1 from control or lalistat-treated THP-1 macrophages incubated for 30 minutes with apoptotic Jurkat cells and cultured for various times and quantification of cleaved caspase-1. (F) Control and lalistat-treated THP-1 macrophages were incubated in the presence or absence of 25 nM Nlrp3 inflammasome inhibitor (CP456773) together with Cell-Tracker Red-prelabeled apoptotic Jurkat cells, and the efferocytic index was quantified by flow cytometry 16 hours later. (G) THP-1 macrophages incubated in the presence or absence of 10 □M lalistat were stimulated with cell tracker Deep Red-prelabeled apoptotic Jurkat cells for 30 minutes. After an additional culture period, the cells were counterstained with Rac1 (green), F-actin (red) and DAPI (nuclear staining); a 3D reconstruction from confocal Z-stack images is provided. (H) Immunoblots of Rac1 from control or lalistat-treated THP-1 macrophages cultured for 3 hours after the ingestion of apoptotic Jurkat cells in presence or absence of 25 nM of the Nlrp3 inflammasome inhibitor (CP-456773). (I) Real-time evaluation of macrophage protrusion dynamics by impedance reading of control or lalistat-treated THP-1 efferocytes in presence or absence of the Rac1 inhibitor, NSC23766. The data are given as the mean ± SEM of two to five independent experiments performed in triplicate. **P*<0.05 *vs.* controls. #*P*<0.05 treatment effect.

Figure 3. Defective lysosomal cholesterol hydrolysis restrains MAM-dependent mitochondrial metabolic repurposing after efferocytosis to activate the inflammasome and subsequent efferocytic defects. (A) Oxygen consumption rate (OCR) recordings of control, lalistat-treated or Lipa over-expressing (Ovex) THP-1 macrophages under the indicated conditions. (B) Representative histograms and (C) quantification of mitochondrial ROS generation using the MitoSox probe by flow cytometry in control and lalistat-treated THP-1 efferocytes cultured for 3 hours after ingestion of apoptotic cells in the presence or absence of 10 mM of the succinate oxidation inhibitor (dimethyl malonate, DMM) or 1μM of the succinate dehydrogenase inhibitor (3-nitropropionic acid, 3-NPA) or 1μM of rotenone. Data are expressed as mean fluorescence intensity (MFI). (D) IL-1β secretion levels in these cells at the end of the incubation period. (E) THP-1 macrophages were transduced with empty or GPR78 overexpressing adenoviral particles and loaded for 30 minutes with the fluorescent calcium probe Fluo4-AM before the start of the efferocytosis experiment. Control and lalistat-treated THP-1 macrophages were then incubated for 30 minutes with apoptotic Jurkat cells before treatment with carbonyl cyanide 3-chlorophenylhydrazone (CCCP) to release mitochondrial calcium. Mitochondrial calcium content was calculated as the difference in mean fluorescence intensity between conditions treated with or without CCCP. (F) Representative transmission electron microscopy images of control or lalistat-treated THP-1 efferocytes showing ER-mitochondria contacts (scale bar, 1 μm). (G) IL-1β secretion levels (H) and efferocytic index from control and GPR78 overexpressing THP-1 macrophages incubated in the presence or absence of 10 μM lalistat and cultured for 3 hours after the ingestion of apoptotic Jurkat cells. The results are expressed as the mean ± SEM of at least two independent experiments performed in triplicate. **P*<0.05 *vs.* controls. #*P*<0.05 treatment effect.

Figure 4. Lysosomal cholesterol hydrolysis governs the efferocytic response by controlling oxysterol production. (A) Oxysterol metabolites (24S-, 4β-, 25- and 27-hydroxy(OH)cholesterol) were determined by liquid chromatography-mass spectrometry (LC-MS). (B) Effects of LIPA inhibition, LIPA overexpression and 25-OHC treatment (5 μM) on *Srebf2* and *Hmgcr* mRNA expression in THP-1 macrophages 3 hours post-efferocytosis. Quantified transcript levels (normalized to m36B4) are expressed in arbitrary units (a.u.). (C) OCR recordings of control and lalistat-treated THP-1 efferocytes in the presence or absence of 5 □M 25-OHC. (D) Control and lalistat-treated THP-1 macrophages, preloaded for 30 minutes with the fluorescent calcium probe Fluo4-AM, were incubated for 30 minutes with apoptotic Jurkat cells in presence or absence of 5 μM 25-OHC. Release of mitochondrial calcium was achieved at the end of the experiment by treating cells with carbonyl cyanide 3-chlorophenylhydrazone (CCCP). Mitochondrial calcium content was calculated as the difference in mean fluorescence intensity between conditions treated with or without CCCP. (E) IL-1β secretion levels from control or lalistat-treated THP-1 efferocytes cultured for 3 hours after the ingestion of apoptotic cells in the presence or absence of 5 μM 25-hydroxycholesterol (25-OHC), 5 μM 27-hydroxycholesterol (27-OHC) or 3 μM LXR agonist (TO901317). (F) Control and lalistat-treated THP-1 macrophages were incubated under the same conditions as described above and the efferocytic index was quantified by flow cytometry 16 hours later. (G). MertK transcript levels (normalized to m36B4) were determined under the same conditions as described in (F) and expressed in arbitrary units (a.u.). (H) Control and lalistat-treated THP-1 macrophages were incubated in the presence or absence of 3 μM LXR agonist (TO901317) and 25 nM Nlrp3 inflammasome inhibitor (CP-456773) together with Cell-Tracker Red-prelabeled apoptotic Jurkat cells and the efferocytic index was quantified by flow cytometry 16 hours later. The results are expressed as the mean ± SEM of two to five independent experiments. **P*<0.05 *vs.* controls. #*P*<0.05 treatment effect.

Figure 5. Inhibition of lysosomal lipid hydrolysis promotes defective efferocytosis in vivo leading to pathogenic inflammation and splenic iron deposition under hypercholesterolemia. (A) Representative dot plots of gating for F4/80^{high}CD11b^{int} KCs, F4/80^{low}CD11b^{high} myeloid cells, and F4/80^{high}CD11b^{high} tMΦ in the liver (top) as well as F4/80^{high}CD11b^{int} RPMs and F4/80^{low}CD11b^{high} myeloid cells in the spleen (bottom) 16 hours after *i.v.* injection of CellTracker^{+} stressed erythrocytes (sRBCs, red) or apoptotic lymphocytes (UV-T, green). Black dot plots represent cells gated on CD45^{+} leukocytes in the liver and

spleen, and the red or green dot plot overlays show CellTracker^{+} cells. Quantification of (B-C) the efferocytic index of each cell type in the liver (myeloid, T-mac and KC) or the spleen (myeloid and RPM). (D) mRNA expression of efferocytic and inflammatory markers in 12-week high-fat-fed WT or *Ldlr*$^{-/-}$ mice treated for the last 2 weeks with subcutaneous injections of either saline or 20 mg/kg lalistat every two days. (E) Perl's Prussian stain for ferric iron in the spleens of these mice (original magnification, 40x and 100x). (F) Iron levels and (G) ferritin levels in spleen, liver and adipose tissue of WT or saline and lalistat-treated *Ldlr*$^{-/-}$ mice on a high-fat diet. The data are expressed as the mean ± SEM of 4 to 6 animals per group. *P<0.05 *vs.* saline-injected control or *Ldlr*$^{-/-}$ mice.

Figure 6. Graphical abstract.

Novelty and Significance

What Is Known?

- Macrophages accumulate a substantial amount of cholesterol following the ingestion of apoptotic cells (ACs).

- LIPA (lysosomal acid lipase) is an endocytic enzyme that hydrolyzes cholesteryl esters into free cholesterol.

- LIPA-deficiency causes macrophage foam cell formation and tissue inflammatory phenotypes.

What New Information Does This Article Contribute?

- LIPA hydrolyzes cholesteryl esters from ingested ACs, allowing efficient oxysterol production to transcriptionally prime macrophages for cholesterol efflux and clearance of ACs via liver X receptor activation.

- LIPA allows 25-hydroxycholesterol generation to repurpose mitochondrial metabolism, preventing activation of the Nlrp3 inflammasome and Rac1-dependent phagocytic cup disassembly.

- LIPA orchestrates disposal of stressed erythrocytes and apoptotic lymphocytes in vivo.

Everyday, billions of dying cells are phagocytosed through efferocytosis to prevent the inflammatory consequences associated with the accumulation of apoptotic debris. Therefore, it has been proposed that defective efferocytosis impairs tissue homeostasis. Here, we found that LIPA-dependent lysosomal cholesterol hydrolysis is essential to maintain an efficient efferocytic response. In vivo, defective clearance of stressed erythrocytes and apoptotic lymphocytes after LIPA inhibition led to an enhanced inflammatory response, culminating in splenomegaly under hypercholesterolemia. Thus, by controlling lysosomal cholesterol hydrolysis, LiPA links the macrophage efferocytic response to chronic inflammation.

Table 1

	Saline-treated Ldr$^{-/-}$	Lalistat-treated Ldr$^{-/-}$
Body weight (g)	24.97 ± 0.32	24.60 ± 1.02
Epididymal adipose tissue (mg)	563 ± 133	485 ± 98
Spleen (mg)	109 ± 13	178 ± 37*
Plasma cholesterol levels (mg/mL)	2.14 ± 0.26	2.18 ± 0.25
Plasma triglyceride levels (mg/mL)	3.69 ± 0.85	4.42 ± 0.19
Plasma ALT levels (U/L)	8.71 ± 1.24	9.77 ± 0.64
Plasma AST levels (U/L)	16.31 ± 3.48	17.63 ± 0.31
Plasma BUN levels (mg/dL)	13.7 ± 3.2	16.5 ± 1.5
Plasma cystatin C levels (mg/L)	0.11 ± 0.01	0.11 ± 0.01
Plasma iron levels (mg/L)	6.19 ± 1.77	6.49 ± 1.44
Plasma ferritin levels (mg/L)	0.34 ± 0.03	0.34 ± 0.01
Plasma IL-1b levels (pg/mL)	*ND*	21.5 ± 5.9
Splenic IL-1b content (pg/mg protein)	114 ± 29	331 ± 37*

Fig. 1

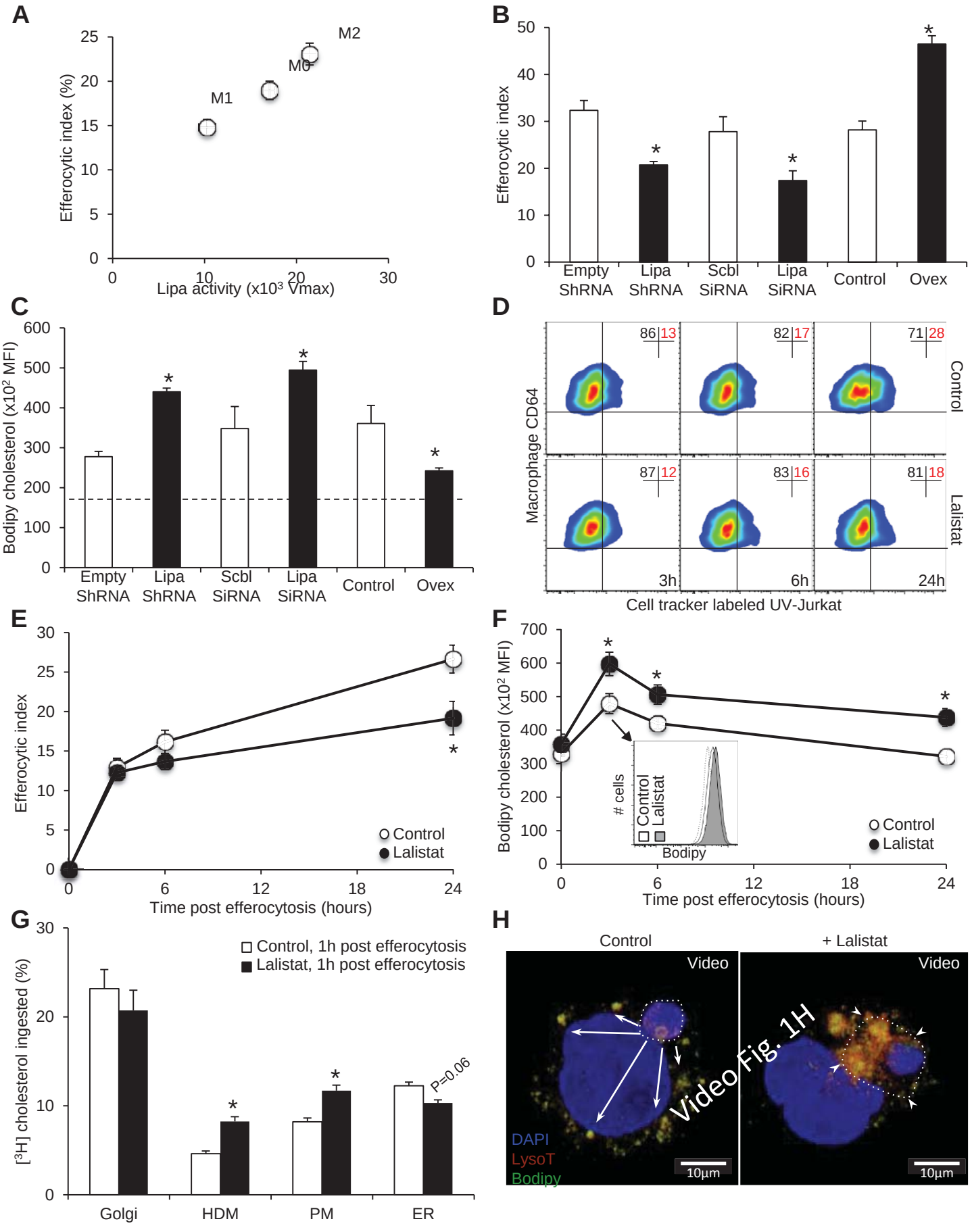

Fig. 2

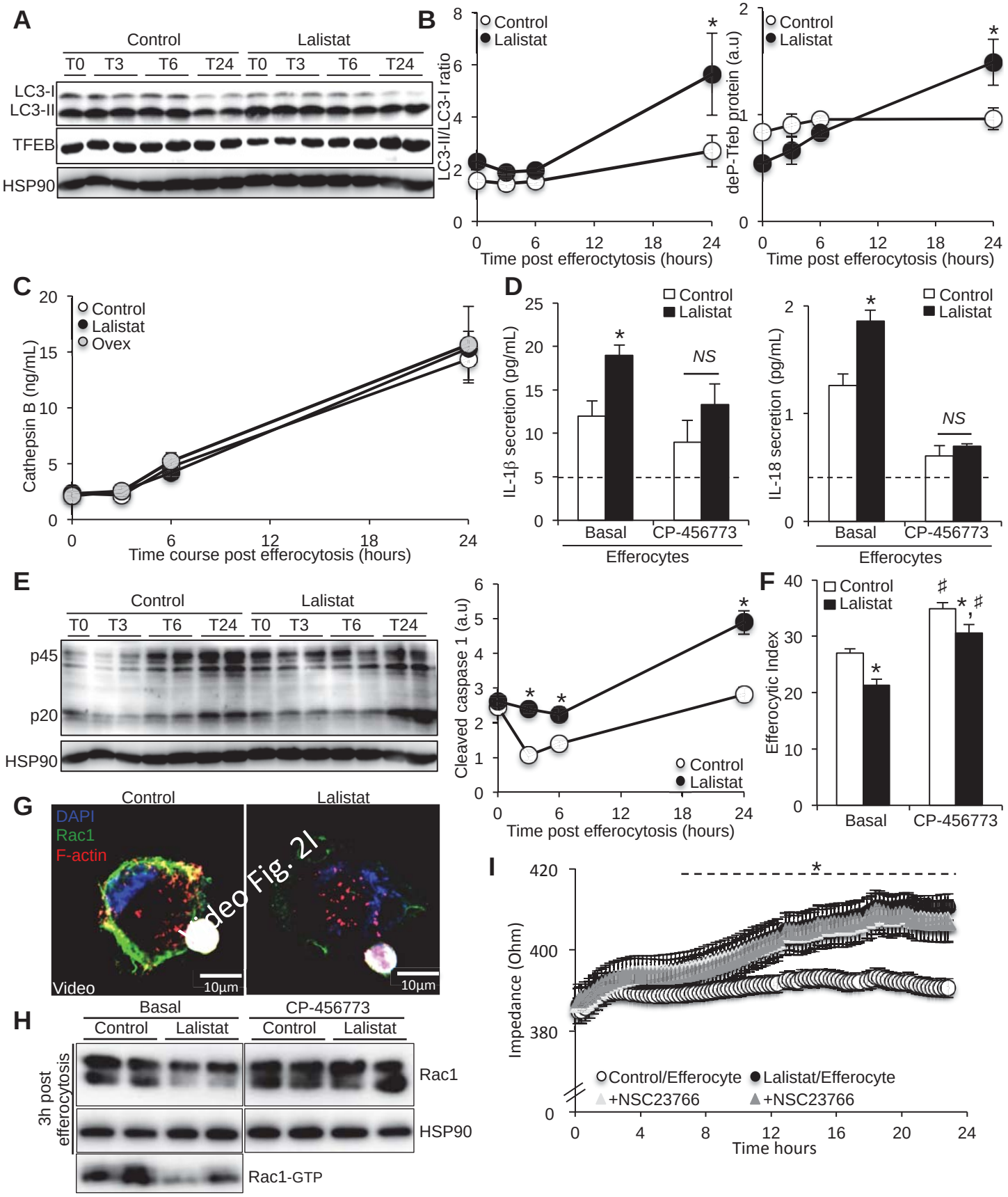

Fig. 3

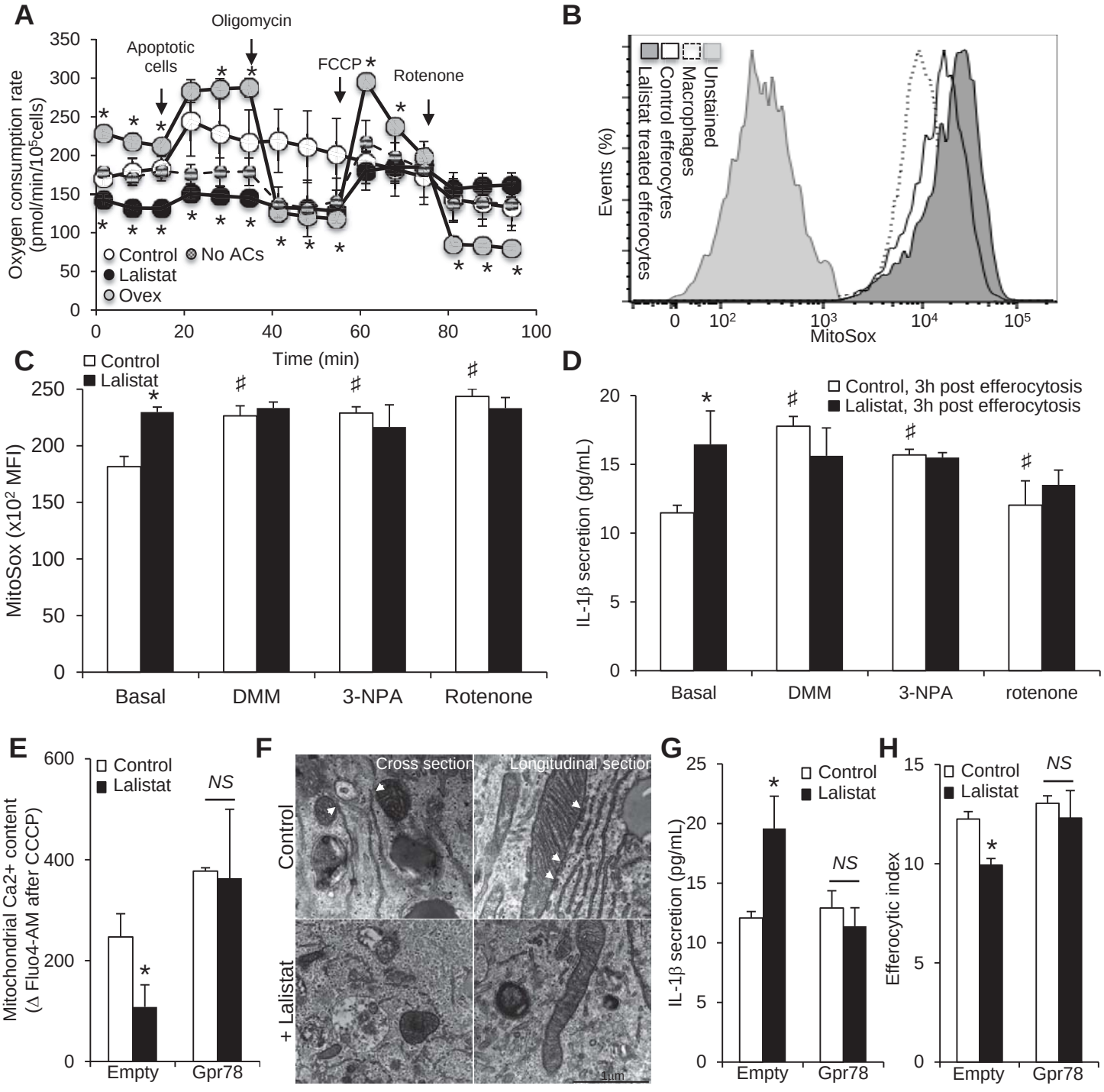

Fig. 4

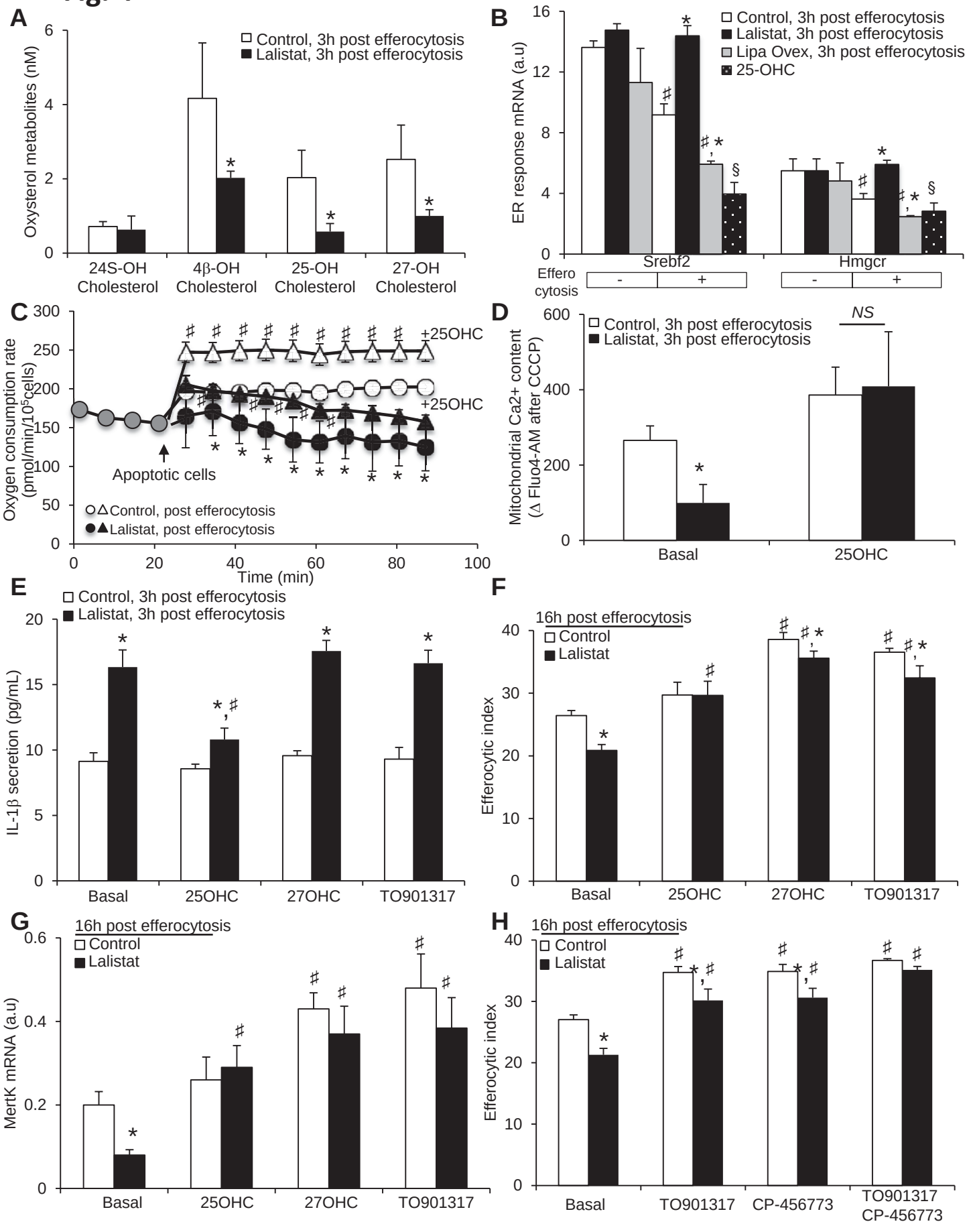

Fig. 5

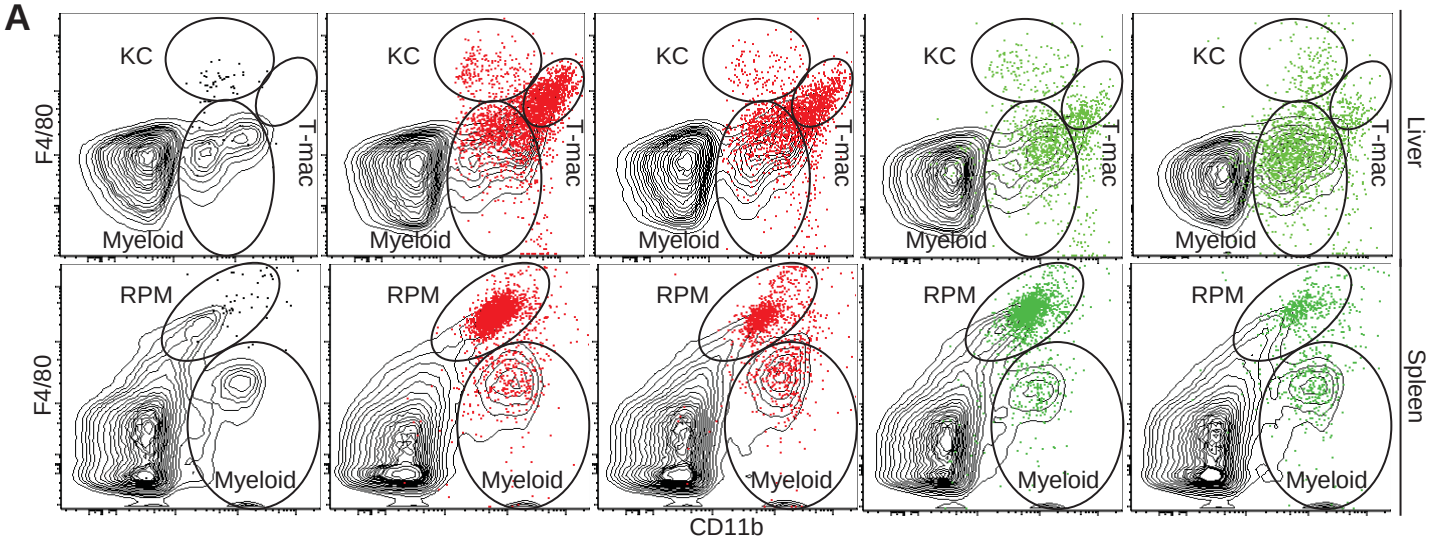

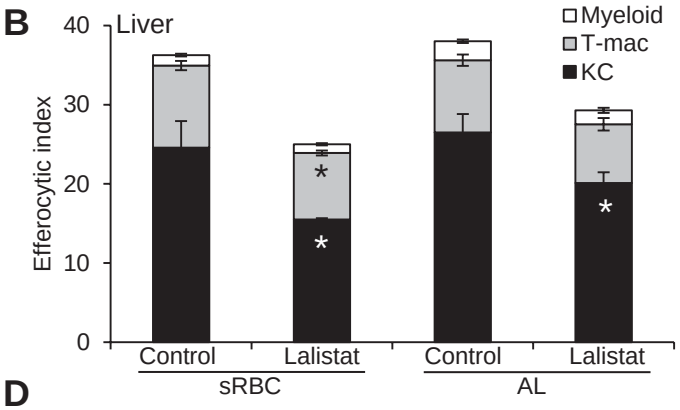

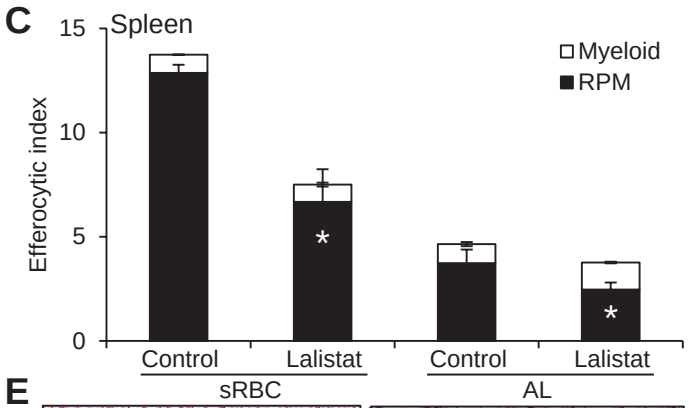

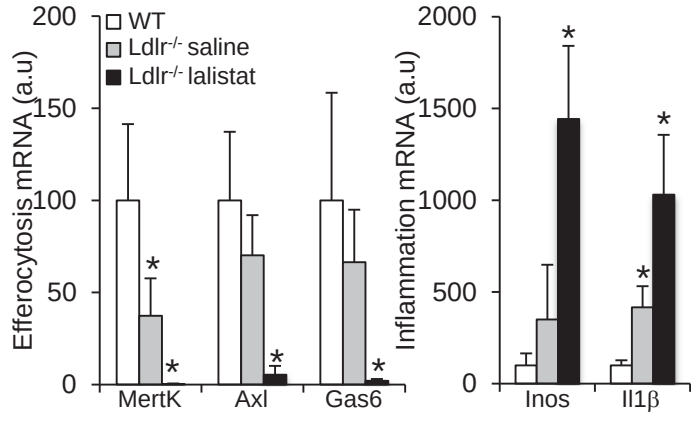

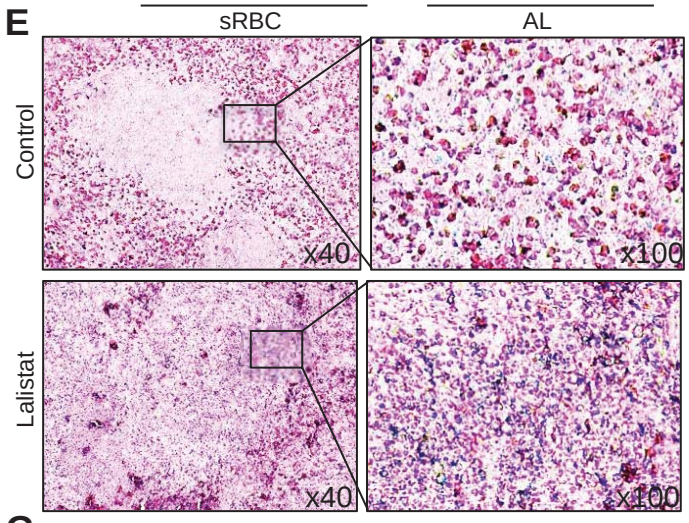

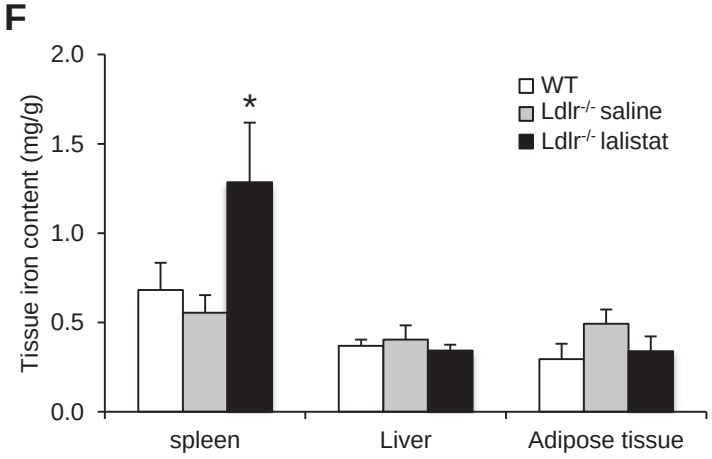

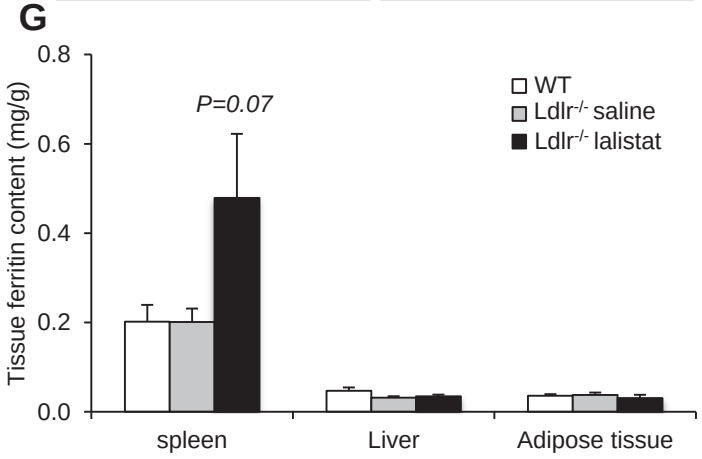

Fig. 6 (Graphical abstract)

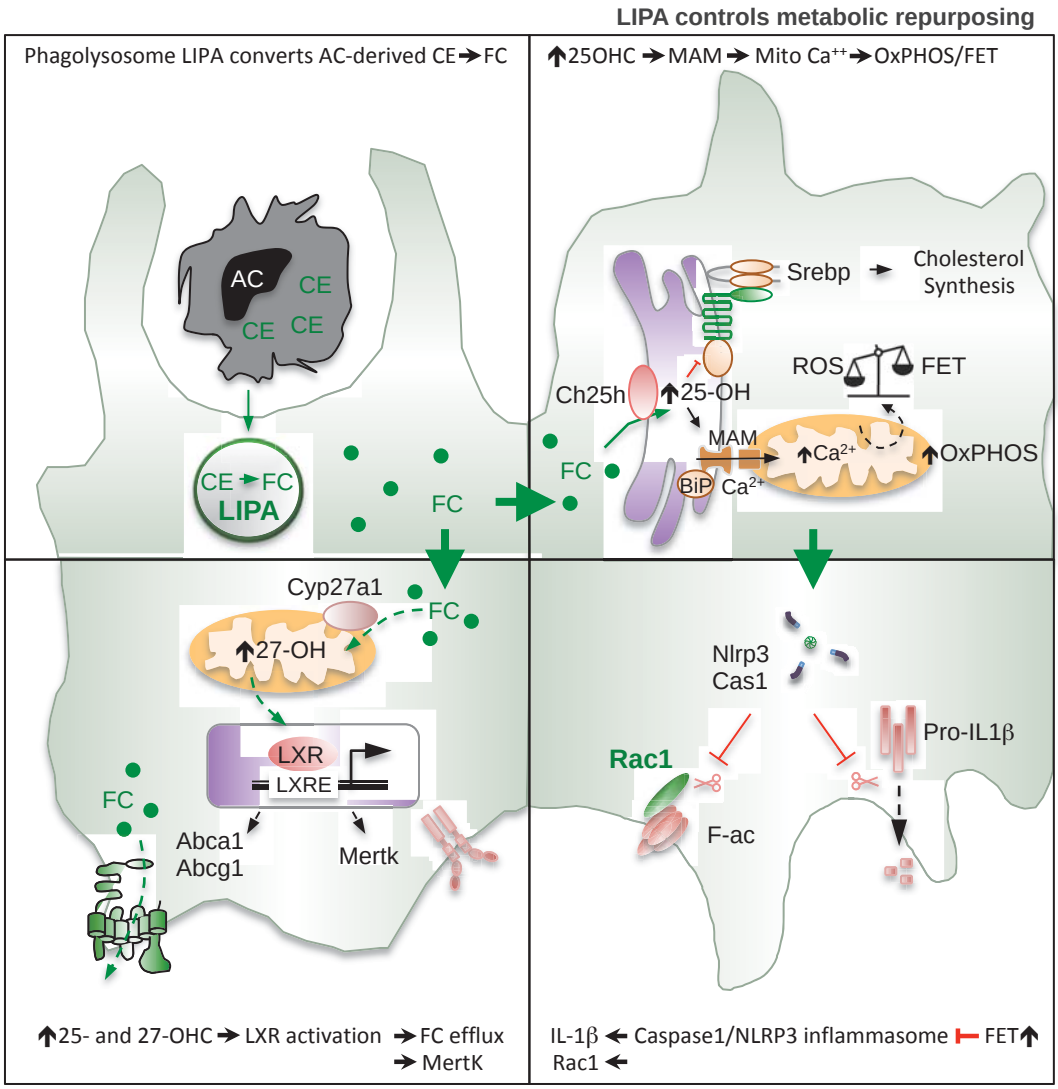

Circulation Research
JOURNAL OF THE AMERICAN HEART ASSOCIATION

Lysosomal Cholesterol Hydrolysis Couples Efferocytosis to Anti-Inflammatory Oxysterol Production

Manon Viaud, Stoyan Ivanov, Nemanja Vujic, Madalina Duta-Mare, Lazaro-Emilio Aira, Thibault Barouillet, Elsa Garcia, François Orange, Isabelle Dugail, Isabelle Hainault, Christian Stehlik, Sandrine Marchetti, Laurent Boyer, Rodolphe Guinamard, Fabienne Foufelle, Andrea E Bochem, Kees G Hovingh, Edward B Thorp, Emmanuel L Gautier, Dagmar Kratky, Paul A Da Silva-Jardine and Laurent Yvan-Charvet

Circ Res. published online March 9, 2018;
Circulation Research is published by the American Heart Association, 7272 Greenville Avenue, Dallas, TX 75231

Print ISSN: 0009-7330. Online ISSN: 1524-4571

Supplement Material

Reagents. Cell culture media and heat-inactivated fetal bovine serum (FBS) were from Invitrogen. Chemical reagents were from Sigma unless specified below. Lalistat was purchased from Enamine ad used as previously described.[1] The antibodies were obtained as follows: $p47^{phox}$ (sc-7660), caspase-1 (sc-1780), LIPA (sc-58374) and hsp90 (sc-13119) from Santa Cruz Biotechnology, Tfeb (A303-673A) from Bethyl Laboratories, LC3-I/II (2775S) from Cell Signaling and Rac1 (610651) from BD Biosciences. Flow cytometry probes were obtained as follows: Bodipy-cholesterol Green and AnnexinV from Life Technologies, FAM-Flica from AbCys Eurobio and Lysosensor Green, LysoTracker^{R} Deep Red, ROS (CM-H2DCFDA), MitoSox and Fluo4-AM from Molecular Probes.

Plasma content analysis. Plasma multi-analyte profiling was performed using a Cobas^{R} clinical chemistry analyzer (Roche Diagnostics).

Plasma HDL preparation. Apo-B containing particles was precipitated from plasma by adding 100µL plasma to 40µL of 20% polyethyleneglycol (PEG, Sigma P-2139 in 200mM glycine, pH 10) solution. This mixture was incubated at room temperature for 15 minutes. After this incubation, the solution was centrifuged at 4,000 rpm for 20 minutes. The supernatant, containing HDL fractions (PEG-HDL), was removed and used for experiments as previously described.[2].

***In vivo* clearance of apoptotic or stressed cells.** To generate apoptotic lymphocytes (ALs), thymi and spleens from 10- to 12- week-old C57BL/6J mice were harvested and mechanistically dissociated, filtered, pelleted and resuspended in DMEM medium supplemented with 10% fetal bovine serum (FBS) (1:1 mixture). Lymphocytes were labelled with Cell-Tracker red (Invitrogen) according to the manufacturer's instructions. Apoptosis was induced by UV radiation at 312nm for 10min and cells were maintained in culture for an additional 2hours. This method results in 70-90% apoptotis.[2] Fluorescent ALs were washed twice with PBS and $6.5x10^{7}$ ALs per mouse were injected intravenously as previously described.[3] A second *in vivo* clearance assay used mice that were injected with stressed red blood cells (sRBCs) as previously described.[4] Briefly, whole blood collected from C57BL/6J mice was pooled, centrifuged at 400*g* for 10min, and the buffy coat was removed. In a second step, RBCs were diluted in PBS and leukoreduced using an adapted Ficoll gradient protocol (Lymphocytes separation medium, AbCys Eurobio). Erythrocytes were labelled with Cell-Tracker red (Invitrogen) according to the manufacturer's instructions. RBCs were then heated for 20min at 48°C under continuous shaking, generating stressed erythrocytes. Fluorescent sRBCs were washed twice with PBS and 400µL of sRBCs adjusted at approximately 16 to 17g/dL of hemoglobin level per mouse were injected intravenously. Mice were sacrificed 16h after injection, and the isolated liver and spleen cells were analyzed by flow cytometry for Cell-Tracker red labeling with up to six mice per group. At this time point, most sRBCs and ALs had disappeared from the circulation. The efferocytic index was determined by flow cyometry and calculated as the number of cells ingested per the total number of macrophages x 100.

***In vivo* flow cytometry analysis.** Leukocytes were collected from spleens, peritoneal cavities, livers and perigonadic adipose tissues. Splenocytes were extracted by pressing spleens through a stainless steel grid. Peritoneal leukocytes were harvested by PBS lavage. Liver and adipose tissue were cut in small piece and digested with 1mg/mL collagenase D (Roche) or collagenase A (Roche) for 30min at 37ºC, respectively. For liver preparation, and additional purification step was performed by Percoll gradient. Single-cell suspension was submitted to red blood cell lysis, filtration and centrifugation for 5min at 1,000rpm. Cell suspensions were stained with the appropriate antibodies for 30min on ice. The following antibodies were used for macrophage flow cytometric analysis: CD45 (30-F11, BD

Bioscience), CD64 (X54-5/7.1, BioLegend), CD11b (M1/70, BioLegend), CD115 (AFS98, BioLegend), CD206 (MR5D3, Bio-Rad) and F4/80 (BM8, BioLegend) using dilution recommended by the manufacturer. Cells were first gated using FSC/SSC characteristics, and doublets were excluded by comparing FSC-height and -area signals. CD45 antibody is used to exclude non-hematopoietic cells. Data were acquired on BD FACS Canto II cytometer and analysed with FlowJo (Tree Star).

Histochemical analysis. Mice were sacrificed and spleen was harvested and fixed in 4% paraformaldehyde. Spleen was embedded in paraffin and 5µm sections were performed using a Microm HM340E microtome (Microm Microtech, Francheville France). Tissue iron distribution was visualized using the Perl's Prussian blue staining method as previously described,[5] and counterstained with eosin.

Tissues and serum iron and ferritin contents. Spleens, livers, perigonadic adipose tissues and serum were analysed for non-heme iron as previously described.[5] Briefly, tissues were weighted and digested in 3M hydrochloric acid/10% trichloroacetic acid, at 65°C for 20h. Iron and ferritin levels were quantified in acid extracts or serum using Cobas^{R} clinical chemistry kits (Roche Diagnostics).

Human THP-1 macrophages and treatments. THP-1 monocytes (TIB-202, ATCC) were cultured in RPMI 1640 medium supplemented with 10% fetal bovine serum (FBS) at 37°C in 5% CO_2. Cells were treated with 100nM PMA (Phorbol myristate acetate) for 3days to facilitate differentiation into macrophages. Adherent cells consisting of macrophages were used for experiments as described in the figure legend in absence or presence of 10µM lalistat during the course of the experiment. The use and concentration of different inhibitors are described in the figure legends. Where indicated, macrophages were incubated for the indicated period of time with 2.5% plasma, 2.5% PEG-HDL, 50ng/mL lipopolysaccharides (LPS, Escherichia coli 0111:B4, Sigma), 20ng/mL IL-4 or apoptotic Jurkat cells (see below). In some experiments, macrophages were incubated with 5 µM 25-hydroxycholesterol (25OHC), 3 µM LXR agonist (TO901317), 5µM 27-hydroxycholesterol (27OHC), 25 nM CP-4567773, 10 mM Dimethyl Malonate (DMM), 1 µM 3-nitropropionic acid (3-NPA), 1µM rotenone, 150 nM cell membrane-permeant derivative of nictotinic acid adenine dinucleotide phosphate (NAADP-AM), 20 µM Mucolipin TRP channel 1 agonist (ML-SA1), 100 µM 2-aminoethyl diphenylborinate (2-ABP) or 50 µM NSC23766 after incubation of the cells with apoptotic Jurkat cells for 30 minutes (see below). RNA interference to suppress CH25H expression was obtained from GE Dharmacon (On-Targetplus Smartpool siRNA) and deliverd into cells using lipofectamine 2000 as previously described in macrophages.[2] Stable LIPA overexpressing THP-1 macrophages and control cells were generated after electroporation of a neomycin resistant pCDN3.3 vector containing human LIPA gene. One out of 7 clones was selected for further analysis based on LIPA expression and activity.

Isolation of mouse peritoneal macrophages. Peritoneal macrophage cells were harvested from WT mice 3 days after receiving an i.p injection of thioglycollate and plated in 10% FBS in DMEM media. After a 1-hour incubation at 37°C, non-adherent cells were removed and adherent cells consisting of macrophages were used for experiment as described in the figure legend. In some experiments, caspase 1 deficient macrophages were used (B6N.129S2-Casp1^{tm1Flv}/J from Jax).

Lipa and Nlrp3 deficient macrophages. Lipa bone marrow cells and immortalized Nlrp3$^{-/-}$ bone marrow cells were kindly provided by Dr. Kratky (Medical University of Gratz, Austria) and Dr. Stelhik (Feinberg School of Medicine, Northwestern University), respectively. Bone-marrow-derived macrophages were cultured in 10% FBS in DMEM media supplemented with macrophage-colony stimulating factor (M-CSF; 20ng/mL; R&D Systems) for 5-10 days before the experiment.[2]

Gpr78 overexpressing macrophages. GRP78 adenoviruses were kindly provided by Dr. Foufelle (Inserm UMRS 1138, Centre de Recherche des Cordeliers). Adenoviruses were amplified in HEK 293 cells and purified on a cesium chloride gradient. THP-1 macrophages were infected at 10 Multiplicity of Infection 48 hours before the start of the experiment.

***In Vitro* Efferocytosis experiments.** Efferocytosis experiments were performed as previously described.[2] Briefly, apoptosis of Jurkat T cells (TIB-152, ATCC) was induced by UV radiation at 312nm for 10min and maintained in culture for 2hours before incubation with macrophages (ratio 5:1) for 30min. For measurement of uptake of apoptotic Jurkat T cells into macrophages, Jurkat T cells were prelabeled with Cell-Tracker red (invitrogen) according to the manufacturer's instructions. The efferocytic index was determined by flow cytometry and calculated as the number of cells ingested per the total number of macrophages x 100. In some experiments, PI was confirmed by microscopy from at least three separate fields (containing ~1,000 cells) from triplicate wells.

Efferocyte cholesterol efflux. Jurkat cells were cultured for 24h in 10%FBS in RPMI containing 1μCi/mL [^{3}H]-cholesterol. Apoptosis of [^{3}H]-cholesterol labelled Jurkat cells was next induced and cells were incubated with human THP-1 macrophages as described above. After 3 extensive washes and an equilibration period of 15min, cholesterol efflux was performed for the indicated period of time in 0.2% BSA RPMI containing 25μg/mL apoA-I or 25μg/mL PEG-HDL. The cholesterol efflux was expressed as the percentage of the radioactivity released from the cells in the medium relative to the total radioactivity in cells plus medium.

Intracellular isotopic cholesterol distribution. A sucrose gradient was prepared by layering 1.98mL of 1.1M sucrose, 1.72mL of 0.88M sucrose, and 1.72mL of 0.58M sucrose in a 6.3mL centrifuge tube. Human THP-1 macrophages ($25x10^6$ cells) incubated for 1hour with [^{3}H]-cholesterol labelled apoptotic Jurkat cells (see protocol above) were collected and homogenized in 2.633mL of low-ionic strength buffer (10mM TrisHCl pH 7.5, 0.5mM $MgCl_2$, 1mM Phenyl Methane Sulfonyl Fluorid, 100U/mL aprotinin). The homogenates were then made isotonic by the addition of 0.527mL of low-ionic strength buffer (1.46M sucrose, 0.3M KCl, 6mM β-Mercapto-Ethanol, 49μM $CaCl_2$, 10mM TrisHCl pH 7.5) and then centrifuged at 10,000g for 15 min at 4°C. The supernatant was divided into two equal portions loaded onto two sucrose density gradient tubes, and centrifuged at 100,000g for 2 hours at 4 °C. This procedure resulted in visible bands at each of the four interfaces plus a pellet as previously described.[6] The pellet, which was enriched in endoplasmic reticulum was washed twice and then resuspended in 150 μl of Buffer A (0.25mM sucrose, 0.15M KCl, 3mM β-Mercapto-Ethanol, 20μM $CaCl_2$, 10mM Tris HCl pH 7.5). The radioactivity was quantified in the five fractions collected and expressed as the percentage of the radioactivity ingested.

Thin-Layer Chromatography (TLC)- Total lipid content was extracted according to the method of Bligh and Dyer. The organic phase containing lipids including the [^{3}H]-cholesterol was collected, evaporated under nitrogen flux and resuspended in 50μL isopropranol. The total amount of extracted lipids was dropped on silica gel POLYGRAM precoated TLC sheets (Sigma). Separation of [^{3}H]-free cholesterol (FC) and [^{3}H]-cholesteryl esters (CE) was achieved in hexane/diethylether/formic acid (80:20:1, v/v/v) running buffer. The radioactivity was quantified and expressed as the percentage of the radioactivity ingested.

Impedance reading of protrusion dynamics. Electric cell-substrate impedance sensing (ECIS) analyser (Applied BioPhysics) was used for real time analysis of morphological changes of intact cells and analysis was performed by ECIS platform (Acquire Innovation). Briefly, human THP-1 monocytes were seeded at $5x10^5$ cells/well in ECIS plates containing gold film electrodes before differentiation into macrophages. After incubation with apoptotic Jurkat cells ($2.5x10^6$ cells/mL), the frequency dependent electrical impedance was measured

in cell-covered electrodes subject to an alternate small electric current. Results were expressed as Ohm normalized to baseline immediately after impedance recordings

Cellular respiration Assays. XPF extracellular flux analyzer (Seahorse Biosciences) was used for real time analysis of the Oxygen Consumption Rate (OCR) of intact cells according to manufacturer's instructions. Briefly, macrophages were seeded at $5x10^5$ cells/well in XPF plates. After incubation with apoptotic Jurkat cells ($2.5x10^6$ cells/mL), efferocytes were treated according to manufacturer's instructions to determine mitochondrial respiration. Results were normalized to the actual cell count immediately after OCR recordings

Lipa activity measurement. LIPA activity was performed as previously described.[7] Briefly, cells were homogenized in 10mM Tris pH8, 50 mM NaCl, 1% Triton X100 buffer containing proteases inhibitors. Protein concentration in cell lysates was determined using a BCA dosage kit (Pearce). A mixture of cell lysate (50μg of protein) was incubated for 30 minutes at 37°C with 250μM of 4-MethylUmbelliferyl Oleate (4-MUO, Sigma) reconstituted in 200mM sodium acetate solution pH 5. To stop the reaction, 1M Tris pH 8 (100μL) was added, and fluorescence intensity was measured.

Rac1 activity assay. Rac1 activity was determined by performing a pull-down of Rac1-GTP (PR-962, Jena Bioscience) according to manufacturer's instructions.

Mitochondrial calcium content. We carried out mitochondrial calcium measurements as previously described,[8] with minor modifications. Briefly, THP-1 macrophages were loaded with 5 μM of the calcium probe Fluo4-AM for 30 minutes at 37°C before the start of the efferocytosis experiments. At the end of the experiment, cells were treated for 10 minutes with 2 μM carbonyl cyanide 3-chlorophenylhydrazone (CCCP), a mitochondrial uncoupler to release mitochondrial calcium and cellular calcium was determined by flow cytometry. Mitochondrial calcium content was calculated as the difference in mean fluorescence intensity between conditions treated with or without CCCP.

Cellular lipid content. Total lipids were extracted with chloroform/methanol from total cell lysates. Cholesterol or triglyceride mass in cells was determined using colorimetric kits (Wako Chemicals).

Directed lipidomic assays. Lipidomic analyses were performed with mass spectrometry by Biocrate Life Sciences using AbsoluteIDQ^R p180-oxysterol assay kit. Briefly, Metabolites from sterol pathway (sterol precursors : lanosterol, 24-dihydrolanosterol, 7-dehydrocholesterol and desmosterol); toxic sterols : alpha triol (cholesterol-3beta, 5alpha, 6beta-triol), alpha epox (cholesterol-5alpha, 6alpha-epoxide), 7alpha-hydroxycholesterol and 7-ketocholesterol; oxysterols : 24S-, 4β-, 25- and 27-hydroxy(OH)cholesterol) were analyzed in human THP-1 efferocytes as indicated in the figure legends. Sterols were extracted according to manufacturer's instructions and analyzed by reversed phase liquid chromatography-mass spectrometry (LC-ECI-MS/MS) to realize liquid chromatography separation, and thus individual quantification of isobaric sterols. The most selective detection was performed in positive MRM detection mode using a SCIEX 4000QTrap tandem mass spectrometry instrument (Applied Biosystems). Data were quantified with Analyst software.

Secretion analysis- Secretion levels of IL1-β, IL-18, Cathepsin D, Cathepsin B and Cathepsin K in human THP-1 macrophages were measured using enzyme-linked immunoabsorbent assay (ELISA) (R&D systems and RayBiotech, Inc.).

***In vitro* flow cytometry assays.** Cells were harvested after trypsin or 5mM EDTA treatment of adherent cells and stained for flow cytometry during 30min at 4°C with labeled antibodies as previously described.[9] Briefly, most of the staining were performed on live cells but for staining performed on fixed cells, one additional step of permeabilization and fixation was

added prior of staining using BD Cytofix/Cytoperm (BD Biosciences) according to manufacturer instructions. Flow cytometry analysis was performed on BD FACS Canto II (BD Biosciences) and analysed with FlowJo (Tree Star). All antibodies were from Biolegend and BD Bioscience and gating strategies are depicted in the Figures. All conditions were performed in triplicates with at least n=3 experiments. Cellular cholesterol content was quantified using the Bodipy-cholesterol probe (Life Technologies), lysosomal content and acidification using the LysoTracker^{R} Deep Red and Lysosensor Green probes (Molecular Probes), Ros production using the CM-H2DCFDA probe (Molecular Probes) and caspase-1 activation was monitored in live cells using the FAM-FLICA assay with the flurosescent FAM-YVAD-FMK probe (Fluorescent Labeled Inhibitor of Caspases) (AbCys Eurobio) according to manufacturer's instructions.

Transmission Electronic Microscopy. Cells were observed with transmission electron microscopy (TEM) for ultrastructural analysis. Cells were fixed in a 1.6 % glutataraldehyde solution in 0.1 M sodium phosphate buffer at room temperature (RT) and stored overnight at 4°C. After three rinsing in 0.1 M cacodylate buffer (15 min each), cells were postfixed in a 1 % osmium tetroxide and 1 % potassium ferrocyanide solution in 0.1 M cacodylate buffer for 1 hour at RT. Cells were subsequently dehydrated in a series of acetone baths (90 %, 100% three times, 15 min each) and progressively embedded in Epon 812 resin (acetone / resin 1:1, 100 % resin two times, 2 hours for each bath). Resin blocs were finally left to harden in a 60 °C oven for 2 days. Ultrathin sections (70 nm) were obtained with a Reichert Ultracut S ultramicrotome equipped with a Drukker International diamond knife and collected on 200 mesh copper grids. Sections were stained with lead citrate and uranyl acetate. TEM observations were performed with a JEOL JEM-1400 transmission electron microscope, equipped with a Morada camera, at a 100 kV acceleration voltage. For analysis of cell adhesive/contact properties, digitized images acquired by TEM were analyzed with ImageJ and data were expressed as percentage of cell contact.

Immunohistochemistry. Human THP-1 macrophages were cultured on coverslips and incubated with the different preparations described below. Cells were then fixed with 4% paraformaldehyde (Sigma) for 15 min at 4°C. Unspecific staining was avoided with a blocking step in PBS 0.1% Triton X100 1% BSA. The coverslips were mounted using Mowiol (Calbiochem) and visualized with a Axioskop 2 FS MOT upright confocal microscope (Nikon 1AR+). Images were obtained by implementing z-scanning, enhanced for publication purposes and analyzed using the ImageJ software as previously described.[2] 3D reconstruction from confocal Z-stack images was also generated. At least three separate fields from triplicate wells for each treatment condition were randomly analyzed.

- *Bodipy-cholesterol diffusion.* UV-induced apoptotic Jurkat cells were stained with 5μM Bopidy-cholesterol for 30min and incubated with THP-1 macrophages for an additional 30min. Then, cells were stained with LysoTracker^{R} Deep Red during 30 minutes at 37°C, as recommended by the manufacturer (Molecular Probes). Cells were washed several times and fixed in 4% formaldehyde solution. Slides were counterstained with DAPI (Sigma). For the quantification of Bopidy-cholesterol in phagolysosome, the mean gray intensity of Bopidy-cholesterol was divided by the mean gray intensity of LysoTracker^{R} Deep Red.

- *Lysosome acidification*. UV-induced apoptotic Jurkat cells were incubated with THP-1 macrophages for 30min as described above and after several washes, 1μM LysoSensor Green was added to cell medium for an additional 30min at 37°C as recommended by the manufacturer's instructions. Cells were washed several times and fixed in 4% formaldehyde solution. Nuclei were counter-stained by addition of DAPI (Sigma). Quantification of LysoSensor Green intensity was performed using the ImageJ software and expressed as mean LysoSensor intensity.

- *p47^{phox} clustering.* Human THP-1 macrophages were incubated with apoptotic Jurkat cells for 30min as described above. Cells were then fixed with 4% paraformaldehyde for 15 min at 4°C and permeabilized with 0.5% Triton for 5min before overnight immunostaining with p47^{phox} antibody as previously described.[2] For the quantification of p47^{phox} in phagolysosome,

the mean gray intensity of $p47^{phox}$ was divided by the mean gray contrast of apoptotic Jurkat cells.
- *Membrane ruffling.* UV-induced apoptotic Jurkat cells were stained with LysoTracker Deep Red for 30min and incubated with THP-1 macrophages for an additional 30min. Then, cells were kept in culture for an additional 30min and washed several times before staining. THP-1 efferocytes were immunostained overnight with Rac1 antibody (Clone 610651, BD Biosciences) in PBS 0,1% Triton X-100, 1% BSA. F-actin was stained with Texas Red-X Phalloidin as recommended by the manufacturer (ThermoScientific). Slides were counterstained with DAPI (Sigma).

Western Blotting. The expression of caspase-1, Nlrp3, Tfeb, LC3-I/II, Rac-1 and LIPA were measured in human THP-1 macrophages or in the cell and supernatant of bone marrow derived macrophages by Western blot analysis. Briefly, cell extracts were electrophoresed on 4-20% gradient SDS-PAGE gels and transferred to 0.22-μm nitrocellulose membranes. The membrane was blocked in Tris-buffered saline, 0.1% Tween20 containing 5%(w/v) nonfat milk (TBST-nfm) at room temperature (RT) for 1h and then incubated with the primary antibody in TBST-nfm at RT for 4h, followed by incubation with the appropriate secondary antibody coupled to horseradish peroxidase. Proteins were detected by ECL chemiluminescence (Pierce). References for primary antibodies are provided in the 'Materials' section. Intensity of each protein strips was quantified using Image J software.

RNA analysis. Total RNA extraction, cDNA synthesis and real-time PCR were performed as described previously.[2] m36B4 RNA expression was used to account for variability in the initial quantities of mRNA.

Statistical analysis
Data are shown as mean ± SEM. Statistical significance was performed using two-tailed parametric student's t test or by one-way analysis of variance (ANOVA, 4-group comparisons) with a Bonferroni multiple comparison post-test according to the dataset (GraphPad software, San Diego, CA). Results were considered as statistically significant when $P<0.05$.

References

1. Rosembaum A, I., Cosner, C.C., Mariani, C.J., Maxfield, F.R., Wiest, O., Helquist, P. (2010). Thiadiazole carbamates: potent inhibitors of lysosomal acid lipase and potential Niemann-Pick type C disease therapeutics. J. Med. Chem. *53*, 5281-9.

2. Yvan-Charvet, L., Pagler, T.A., Seimon, T.A., Thorp, E., Welch, C.L., Witztum, J.L., Tabas, I., and Tall, A.R. (2010). ABCA1 and ABCG1 protect against oxidative stress-induced macrophage apoptosis during efferocytosis. Circ. Res. *106*, 1861–1869.

3. Scott, R.S., McMahon, E.J., Pop, S.M., Reap, E.A., Caricchio, R., Cohen, P.L., Earp, H.S., and Matsushima, G.K. (2001). Phagocytosis and clearance of apoptotic cells is mediated by MER. Nature *411*, 207–211.

4. Theurl, I., Hilgendorf, I., Nairz, M., Tymoszuk, P., Haschka, D., Asshoff, M., He, S., Gerhardt, L.M.S., Holderried, T.A.W., Seifert, M., et al. (2016). On-demand erythrocyte disposal and iron recycling requires transient macrophages in the liver. Nat. Med. *22*, 945–951.

5. Kohyama, M., Ise, W., Edelson, B.T., Wilker, P.R., Hildner, K., Mejia, C., Frazier, W.A., Murphy, T.L., and Murphy, K.M. (2009). Role for Spi-C in the development of red pulp macrophages and splenic iron homeostasis. Nature *457*, 318–321.

6. Li, Y., Ge, M., Ciani, L., Kuriakose, G., Westover, E.J., Dura, M., Covey, D.F., Freed, J.H., Maxfield, F.R., Lytton, J., et al. (2004). Enrichment of endoplasmic reticulum with cholesterol inhibits sarcoplasmic-endoplasmic reticulum calcium ATPase-2b activity in parallel with increased order of membrane lipids: implications for depletion of endoplasmic reticulum calcium stores and apoptosis in cholesterol-loaded macrophages. J. Biol. Chem. *279*, 37030–37039.

7. Emanuel, R., Sergin, I., Bhattacharya, S., Turner, J.N., Epelman, S., Settembre, C., Diwan, A., Ballabio, A., and Razani, B. (2014). Induction of lysosomal biogenesis in atherosclerotic macrophages can rescue lipid-induced lysosomal dysfunction and downstream sequelae. Arterioscler. Thromb. Vasc. Biol. *34*, 1942–1952.

8. Lloyd-Evans, E., Morgan, A., He, X., Smith, D.A., Elliot-Smith, E., Sillence, D.J., Churchill, G.C., Schuchman, E.H., Galione, A., Platt, F.M. (2008). Niemann-Pick disease type C1 is a sphingosine storage disease that causes deregulation of lysosomal calcium. Nat Med. *14*, 1247-55.

9. Sarrazy, V., Sore, S., Viaud, M., Rignol, G., Westerterp, M., Ceppo, F., Tanti, J.-F., Guinamard, R., Gautier, E.L., and Yvan-Charvet, L. (2015). Maintenance of Macrophage Redox Status by ChREBP Limits Inflammation and Apoptosis and Protects against Advanced Atherosclerotic Lesion Formation. Cell Rep *13*, 132–144.

Supplemental Figure I. Defective lysosomal cholesterol hydrolysis promotes lysosomal cholesterol accumulation during efferocytosis. (A) Lysosomal acid lipase (LIPA) mRNA expression (normalized to m36B4) was determined by real-time polymerase chain reaction (PCR) in human THP-1 macrophages after LIPA knockdown (using lentiviral ShRNA particles or siRNA) or after LIPA inhibition achieved with 10 μM lalistat. (B, upper panel) Immunoblot of LIPA from control and LIPA-overexpressing THP-1 macrophages (LIPA Ovex) generated by lentiviral transfection. LIPA Ovex THP-1 macrophage clone #2 was selected for further analysis. (B, lower panel) LIPA activity from control, lalistat-treated and LIPA-overexpressing (clone #2) THP-1 macrophages. Enzymatic activity (normalized to control DMSO) was quantified at acidic pH at 37°C after the reaction was initiated by adding 250 μM 4MUO substrate and monitored for 30 minutes. (C) WT and Lipa deficient bone marrow-derived macrophages were incubated for the indicated times in the presence or absence of 10 μM lalistat together with Cell-Tracker Deep Red-prelabeled apoptotic Jurkat cells, and the efferocytic index was quantified by flow cytometry. (D) WT and Lipa deficient bone marrow-derived macrophages incubated in the presence or absence of 10 μM lalistat were stimulated with apoptotic Jurkat cells for the indicated times. BODIPY staining was quantified by flow cytometry. (E) Control and LIPA-overexpressing THP-1 efferocytes, cultured for 1 hour after the ingestion of [^{3}H]-cholesterol-prelabeled apoptotic Jurkat cells, were fractionated by sucrose step gradient, and fractions were assayed for [^{3}H]-cholesterol incorporation as described in the Methods section. (F) Quantification of [^{3}H]-free cholesterol (FC) and cholesteryl ester (CE) incorporation by thin-layer chromatography (TLC) in high-density membrane (HDM) containing lysosomes, plasma membrane (PM) and endoplasmic reticulum (ER) of control or lalistat-treated THP-1 efferocytes 1 hour after the ingestion of [^{3}H]-cholesterol-prelabeled apoptotic Jurkat cells. (G) Representative images of transmission electron microscopy of control or lalistat-treated THP-1 macrophages (eight to ten different transmission electron microscopy images from individual cells with over four hundred lysosomes were analyzed per condition) showing higher lysosome numbers with similar structures (left panels). Lysosomal membrane structure including 'onion-ring' or 'whorl-shaped' phospholipid-rich lysosomes is shown in control cells (upper right panels) and cholesterol crystal-containing lysosomes is shown in lalistat-treated cells (lower right panel; 1 identified among more than 400 visualized lysosomes) (scale bar, 5 and 1 μm). (H) Control, lalistat-treated and LIPA Ovex THP-1 macrophages were stimulated with BODIPY green-prelabeled apoptotic Jurkat cells for 30 minutes. The cells were counterstained with LysoTracker^R Deep Red (phagolysosome staining) and DAPI (nuclear staining), and representative confocal images (magnification 80x and 160x) are depicted (eight to ten different confocal images were analyzed per condition from experiments performed in triplicate). The data represent the averages ± SEM of at least three independent experiments. *P<0.05 *vs.* controls.

Supplemental Figure II. Defective lysosomal cholesterol hydrolysis does not initiate phagolysosome dysfunction but promotes lysosomal biogenesis after efferocytosis to prevent cell from apoptosis. (A) Representative immunoblots of LC3I/II and phospho-Tfeb from control or LIPA overexpressing (Ovex) THP-1 macrophages incubated for 30 minutes with apoptotic Jurkat cells and cultured for various times. (B) Visualization of the phagolysosome (gray contrast) surrounding p47^{phox} staining after performing 3D reconstruction from confocal Z-stack images of an ingested apoptotic cell. Quantification of p47^{phox} in phagolysosomes 1 hour post-efferocytosis was performed as described in the Methods section with the use of ImageJ software. (C) Confocal analysis of LysoSensor-stained (green) control or lalistat-treated THP-1 macrophages exposed to apoptotic Jurkat cells for 1 hour. Cells were counterstained with DAPI (nuclear staining). The quantification of LysoSensor fluorescence intensity was performed as described in the Methods section with the use of ImageJ software. **(**D) The lysosomal acidification of control, lalistat-treated or LIPA-Ovex THP-1 efferocytes was analyzed by flow cytometry with the fluorescent LysoSensor probe at the indicated time points and was expressed as the mean fluorescence intensity (MFI). (E) Flow cytometry analysis of fluorescent LysoTracker^R Deep Red at the

indicated time points and expressed as the mean fluorescence intensity (MFI) in control, lalistat-treated or LIPA-Ovex efferocytes. (F). The percentage of apoptosis was determined using the Annexin V probe by flow cytometry in THP-1 macrophages after LIPA knockdown (using lentiviral ShRNA particles or siRNA), LIPA inhibition (10 μM lalistat treatment) or LIPA overexpression (Ovex) and exposure to apoptotic cells for 16 hours. The data are given as the mean ± SEM from three independent experiments. *P<0.05 *vs.* controls.

Supplemental Figure III. Defective lysosomal cholesterol hydrolysis activates the NLRP3 inflammasome and promotes Rac1-dependent phagocytic cup disassembly. (A) Cathepsin K secretion levels from control or lalistat-treated THP-1 efferocytes cultured for the indicated times after the ingestion of apoptotic cells were measured and expressed in pmol/L. (B) IL-1β secretion levels (expressed in pg/mL) from control or lalistat-treated murine thyoglycollate-elicited peritoneal macrophages cultured for 16 hours after the ingestion of apoptotic cells. (C) IL-1β secretion levels from control or LIPA overexpressing (Ovex) THP-1 efferocytes cultured for the indicated times after the ingestion of apoptotic cells were measured and expressed in pg/mL. (D) Caspase-1 activity determined by flow cytometry with the FAM-FLICA assay kit in control and lalistat-treated THP-1 efferocytes cultured for 16 hours after the ingestion of apoptotic cells in the presence or absence of 25 nM of the Nlrp3 inflammasome inhibitor (CP-456773). The data are expressed as the mean fluorescence intensity (MFI). (E) IL-1β secretion levels from control and immortalized Nlrp3$^{-/-}$ bone marrow-derived macrophages incubated in the presence or absence of 10 μM lalistat and cultured for an additional 16 hours after the ingestion of apoptotic Jurkat cells. (F) Treatment of control and Nlrp3$^{-/-}$ bone marrow-derived efferocytes in the presence or absence of 10 μM lalistat and cultured for 16 hours. Caspase-1 cleavage was quantified by Western blot. (G) Control and lalistat-treated thyoglycollate-elicited peritoneal macrophages isolated from WT or caspase 1 deficient mice were incubated in the presence or absence of 25 nM Nlrp3 inflammasome inhibitor (CP456773) together with Cell-Tracker Red-prelabeled apoptotic Jurkat cells, and the efferocytic index was quantified by flow cytometry 16 hours later. (H) Representative transmission electron microscopy images of control or lalistat-treated THP-1 efferocytes showing membrane structure (scale bar, 20 μm). (I) THP-1 macrophages incubated in the presence or absence of 10 μM lalistat were stimulated with cell tracker Deep Red-prelabeled apoptotic Jurkat cells for 30 minutes. After an additional culture period, the cells were counterstained with Rac1 (green), F-actin (red) and DAPI (nuclear staining); representative confocal images are depicted (eight to ten different confocal images were analyzed per condition from experiments performed in triplicate). The results are expressed as the mean ± SEM of at least two experiments performed in triplicate. *P<0.05 *vs.* controls.

Supplemental Figure IV. Impaired mitochondrial metabolic repurposing but not lysosomal calcium release is the culprit of the inflammasome activation after LIPA inhibition. (A) Oxygen consumption rate (OCR) recordings of control or lalistat-treated THP-1 macrophages incubated with apoptotic Jurkat cells for the indicated times. The OCR of apoptotic Jurkat cells was also recorded. (B) OCR of control or lalistat-treated thyoglycollate-elicited murine peritoneal macrophages in presence or absence of apoptotic Jurkat cells and in Lipa deficient efferocytes. (C-D) mRNA expression of *Ucp-2* and *Hmox1* in control or lalistat-treated THP-1 efferocytes at the indicated time points. The expression of mRNA was normalized to m36B4 and expressed in arbitrary units (a.u.). (E) Caspase-1 activity determined by flow cytometry with the FAM-FLICA assay kit in control and lalistat-treated THP-1 efferocytes cultured for 3 hours after ingestion of apoptotic cells in the presence or absence of 150 nM of the cell membrane-permeant derivative of nictotinic acid adenine dinucleotide phosphate (NAADP-AM), 20 μM of the lysosomal Mucolipin TRP channel 1 agonist (ML-SA1) that release calcium from the acidic compartment or 10 μM of 2-aminoethyl diphenylborinate (2-APB), a membrane permeable IP3 receptor modulator that stimulates store-operated calcium release at 10 μM concentration. Data are expressed as mean fluorescence intensity (MFI). (F) IL-1β secretion levels in these cells at the end of the

incubation period. The results are expressed as the mean ± SEM of at least two independent experiments performed in triplicate. *P<0.05 *vs.* controls.

Supplemental Figure V. LIPA favors the generation of 25-OHC during efferocytosis to down-regulate the expression of cholesterol biosynthesis genes and prevent activation of the inflammasome. Effect of LIPA inhibition on (A) sterol precursors (lanosterol, 24-dihydrolanosterol, 7-dehydrocholesterol and desmosterol) and (B) toxic sterols (alpha-triol (cholesterane-3beta,5alpha,6beta-triol), alpha-epox (cholesterol-5alpha, 6alpha-epoxide), 7alpha-hydroxycholesterol and 7-ketocholesterol) determined by liquid chromatography-mass spectrometry (LC-MS) in THP-1 macrophages 3 hours post-efferocytosis. (B) mRNA expression of oxysterol-producing enzymes in THP-1 macrophages 3 hours post-efferocytosis. (D-E) Transcript levels of endoplasmic cholesterol biosynthesis genes (*Srebf2* and *Hmgcr*) in control or lalistat-treated THP-1 efferocytes at the indicated time points. Quantified transcript levels (normalized to m36B4) are expressed in arbitrary units (a.u.). (F) WT and Lipa deficient murine efferocytes were incubated in the presence or absence of 5 μM 25-hydroxycholesterol (25-OHC) and the efferocytic index was quantified by flow cytometry 16 hours later. (G) LIPA-overexpressing (Ovex) THP-1 macrophages treated with scrambled or *Ch25h* SiRNA were incubated for 30 minutes with apoptotic Jurkat cells, extensively washed, and cultured for an additional 16 hours. Ch25h mRNA expression, normalized to m36B4, was expressed in arbitrary units (a.u.) and IL-1β secretion levels were expressed in pg/mL. The results are expressed as the mean ± SEM of two to five independent experiments performed in triplicate. *P<0.05 *vs.* controls. #P<0.05 treatment effect.

Supplemental Figure VI. LIPA induces liver X receptor (LXR) activation during efferocytosis. (A-B) THP-1 macrophages were incubated for the indicated times in the presence or absence of 10 μM lalistat together with apoptotic Jurkat cells, and the transcript levels of *Abca1* and *Abcg1* (normalized to m36B4) were determined by real-time polymerase chain reaction (PCR; n=3). (C-D) THP-1 macrophages were incubated for 30 minutes in the presence or absence of 10 μM lalistat together with [^{3}H]-cholesterol-prelabeled apoptotic Jurkat cells. Then, apoA-I or polyethylene glycol (PEG)-HDL was added as an acceptor and incubated for 6 or 24 hours before the media and cells were collected for isotopic cholesterol efflux analysis. (E) Control and LIPA Ovex THP-1 macrophages were incubated in the presence or absence of apoptotic Jurkat cells for 30 minutes, extensively washed, and cultured for an additional 24 hours. At the end of the incubation, *Abca1*, *Abcg1* and *MertK* transcript levels (normalized to m36B4) were quantified and expressed in arbitrary units (a.u). (F) Control and LIPA Ovex THP-1 macrophages were incubated for 30 minutes with [^{3}H]-cholesterol-prelabeled apoptotic Jurkat cells. After an equilibration period, polyethylene glycol (PEG)-HDL was added as an acceptor and incubated for 6 or 24 hours before the media and cells were collected for isotopic cholesterol efflux analysis. (G) mRNA expression of LXR target genes (*Abca1* and *Abcg1*) in control or lalistat-treated THP-1 macrophages 24 hours after efferocytosis in the presence or absence of 3 μM LXR agonist (TO901317). The expression of mRNA was normalized to m36B4 and expressed in arbitrary units (a.u). (H) THP-1 macrophages were incubated for 30 minutes in the presence or absence of 10 μM lalistat or 3 μM LXR agonist (TO901317) together with [^{3}H]-cholesterol-prelabeled apoptotic Jurkat cells. Then, polyethylene glycol (PEG)-HDL was added as an acceptor and incubated for 24 hours before the media and cells were collected for isotopic cholesterol efflux analysis. The data are given as the mean ± SEM from three independent experiments. *P<0.05 *vs.* controls. #P<0.05 treatment effect.

Supplemental Figure VII. Targeted gene expression profiling of LIPA and related lysosomal and efferocytic functions in tissue-resident immune cells and effects of LIPA inhibition on the efferocytosis of stressed erythrocytes and apoptotic lymphocytes. (A) Heat map of LIPA, lysosomal and efferocytic functions, LXR target genes,

heme/iron metabolism and inflammasome markers in various hematopoietic, lymphoid and myeloid cell populations generated from a publicly available Immgen dataset. (B) Representative dot plots showing the uptake of CellTracker^{+} stressed erythrocytes (sRBCs, red) or apoptotic lymphocytes (UV-T, green) in the liver (top) and spleen (bottom) 16 hours after *i.v.* injection. (C-D) Quantification of the percentage of efferocytic cells of each cell type in the liver (myeloid, T-mac and KC) or the spleen (myeloid and RPM). The results are expressed as the mean ± SEM of 4 to 6 animals per group. *P<0.05 *vs.* saline-injected control mice.

Supplemental Figure VIII. Inhibition of lysosomal lipid hydrolysis promotes pathogenic tissue-resident macrophage expansion and lysosomal dysfunction. (A) Representative dot plots of tissue-resident macrophages (F4/80^{+}CD64^{+} splenic RPMs, liver KCs and adipose tissue ATMs and F4/80^{+}CD115^{+} peritoneal PCMs) by flow cytometry from 12-week high-fat-fed WT or *Ldlr*$^{-/-}$ mice treated for the last 2 weeks with subcutaneous injections of either saline or 20 mg/kg lalistat every two days. (B) Quantification of tissue-resident macrophages expressed as a percentage of whole tissue. (C) Representative histograms and quantification of CD206 cell surface expression in splenic RPMs by flow cytometry and expressed as the mean fluorescence intensity (MFI). (D) Lysosomal content and acidification in tissue-resident macrophages quantified by flow cytometry using LysoTracker^{R} Deep Red and LysoSensor Green, respectively, and expressed as the mean fluorescence intensity (MFI). The results expressed as are the mean ± SEM from 4 to 6 animals per group. *P<0.05 *vs.* saline injected *Ldlr*$^{-/-}$ mice.

Supplemental Figure I.

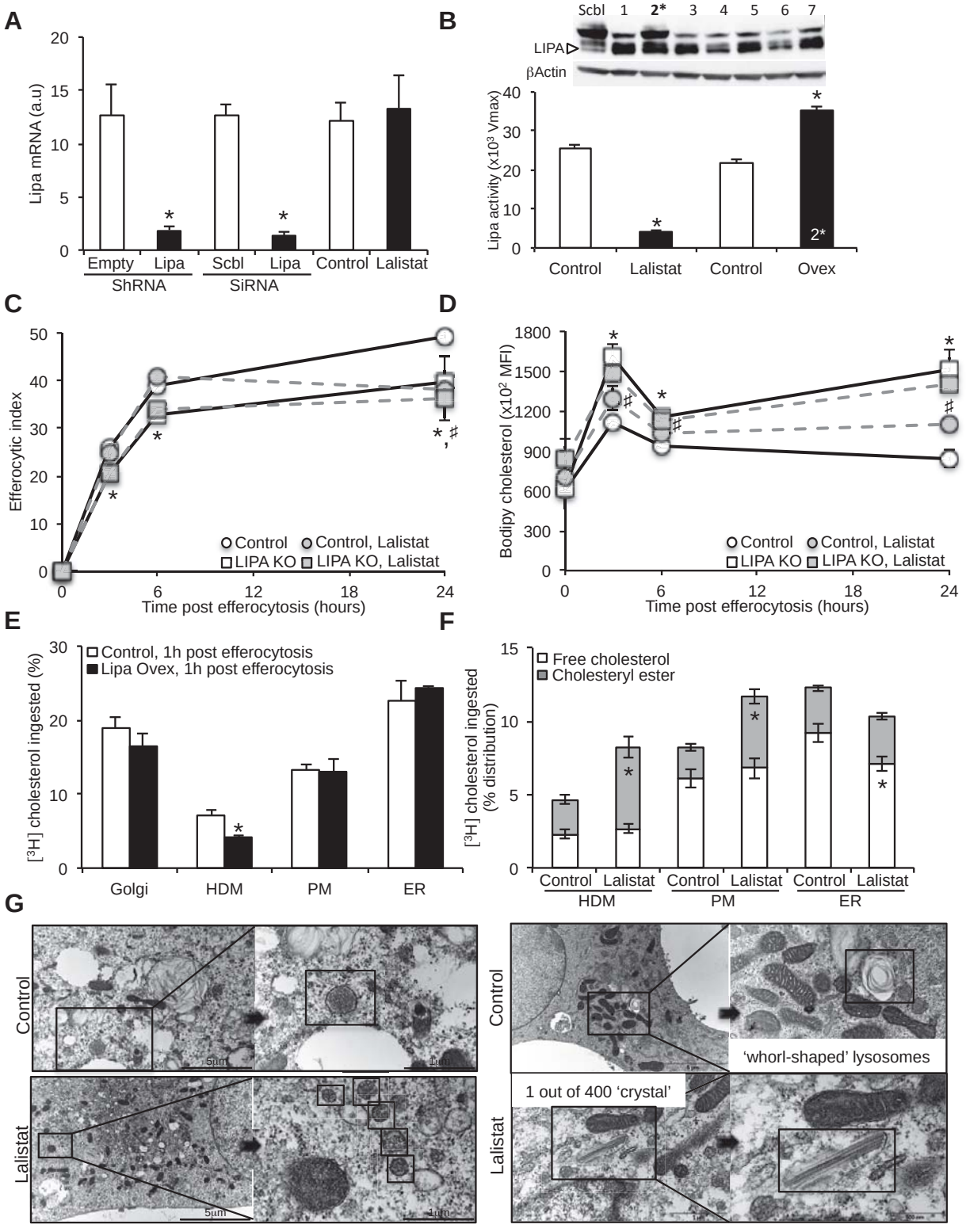

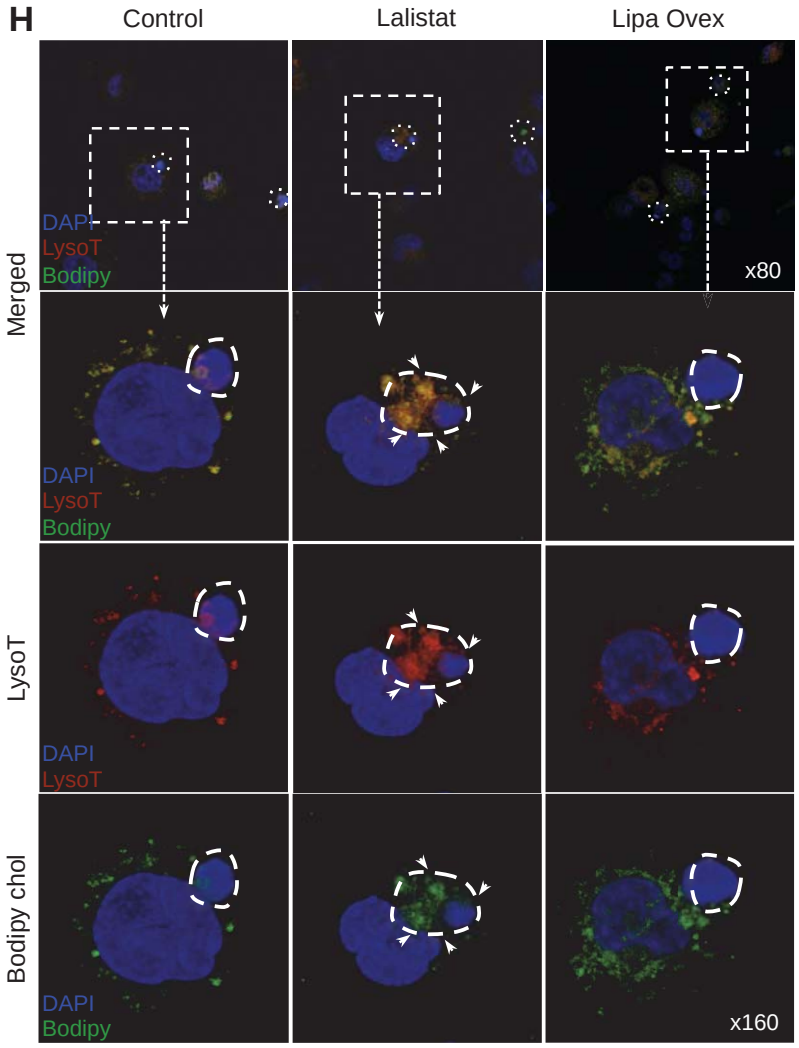
H
Control
Lalistat
Lipa Ovex
Merged
LysoT
Bodipy chol
DAPI
LysoT
Bodipy
x80
x160

Supplemental Figure II.

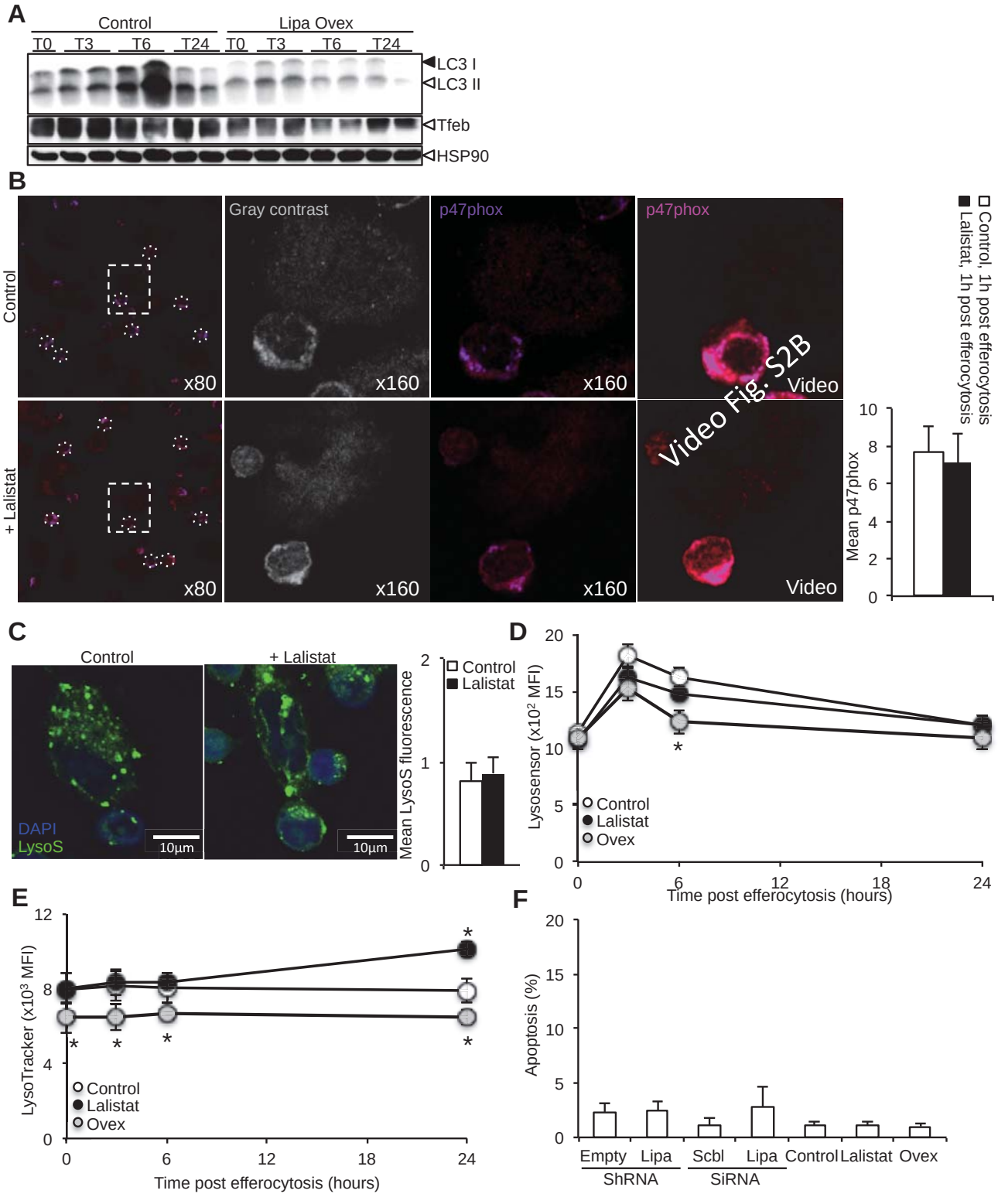

Supplemental Figure III.

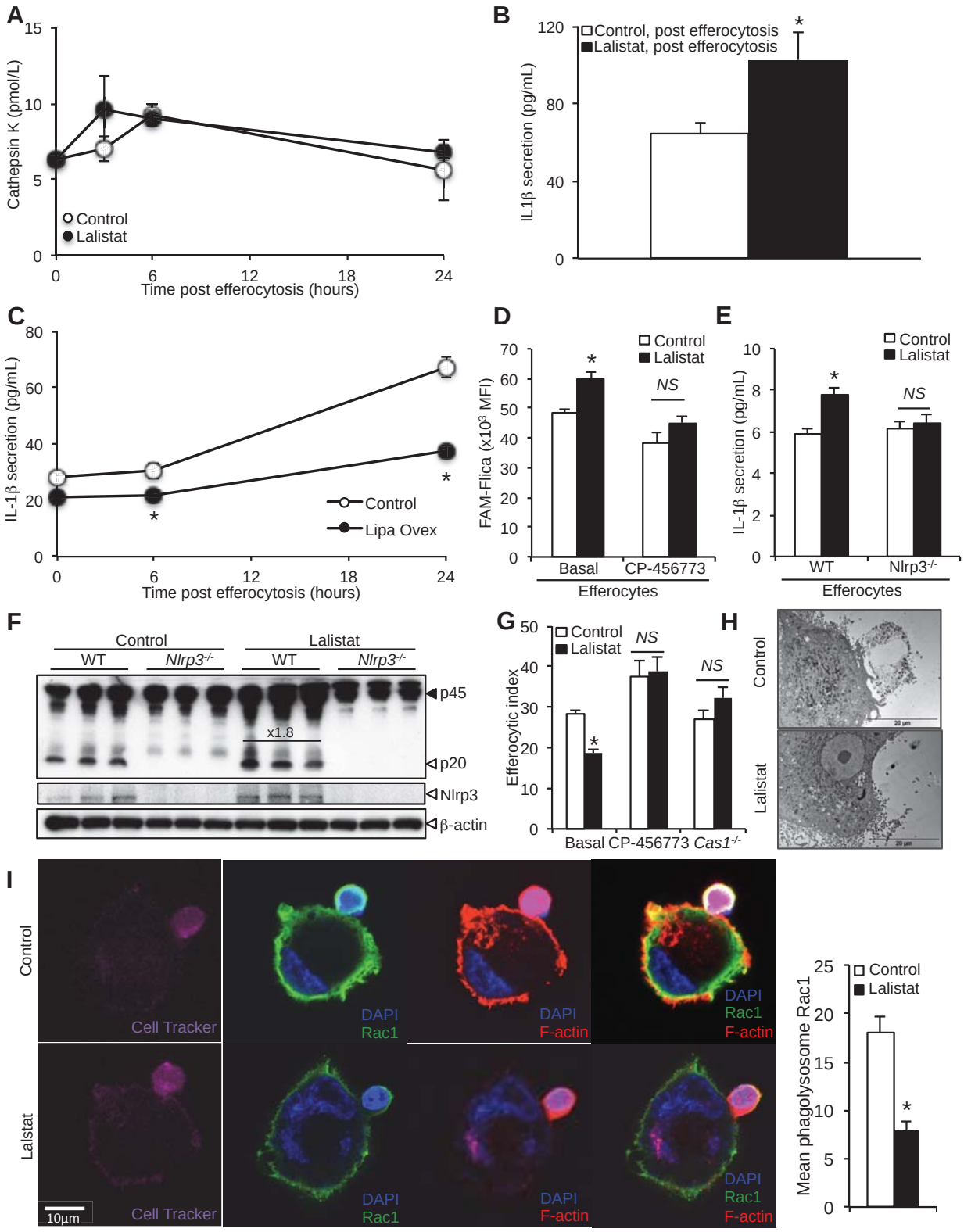

Supplemental Figure IV.

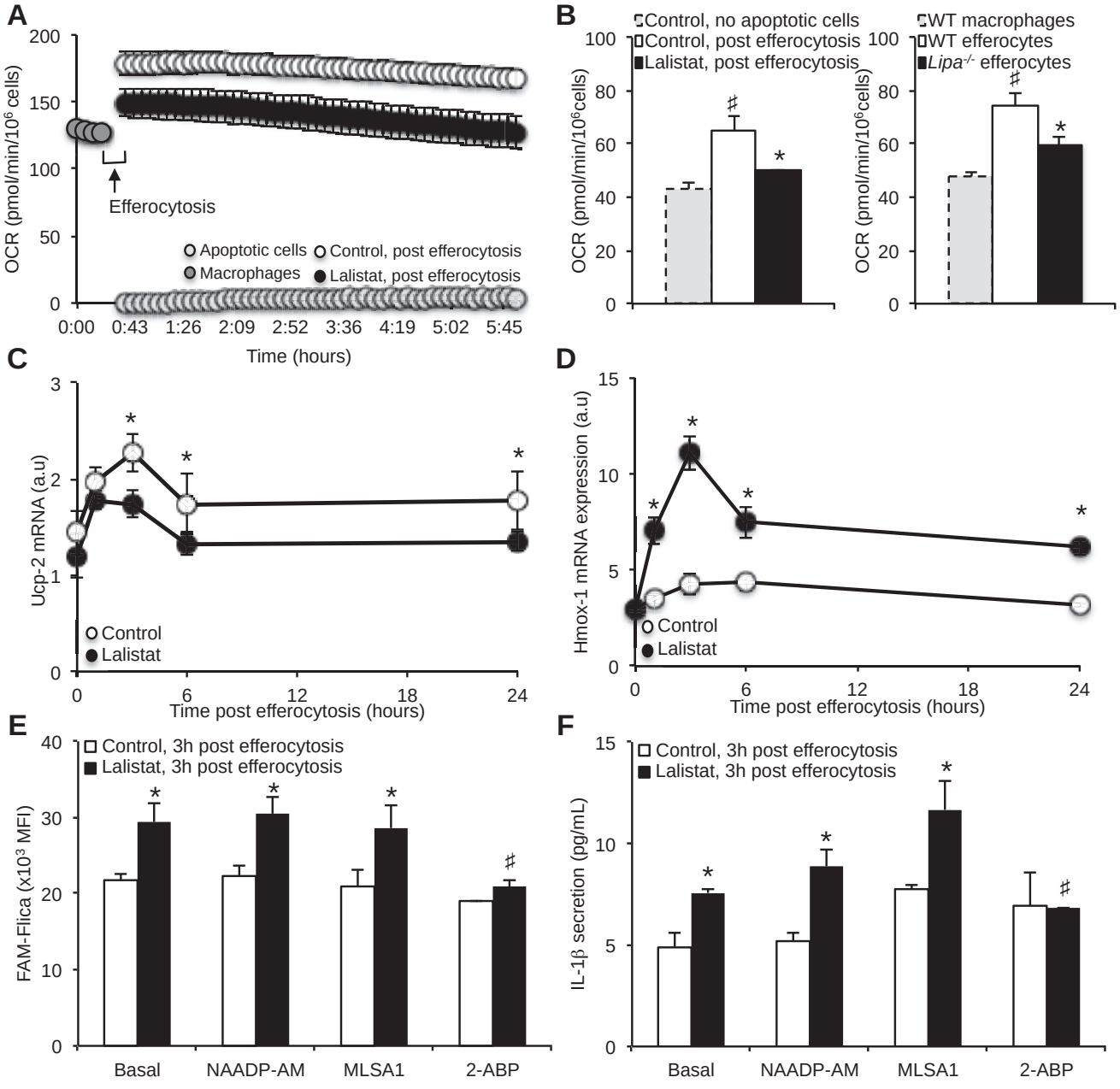

Supplemental Figure V.

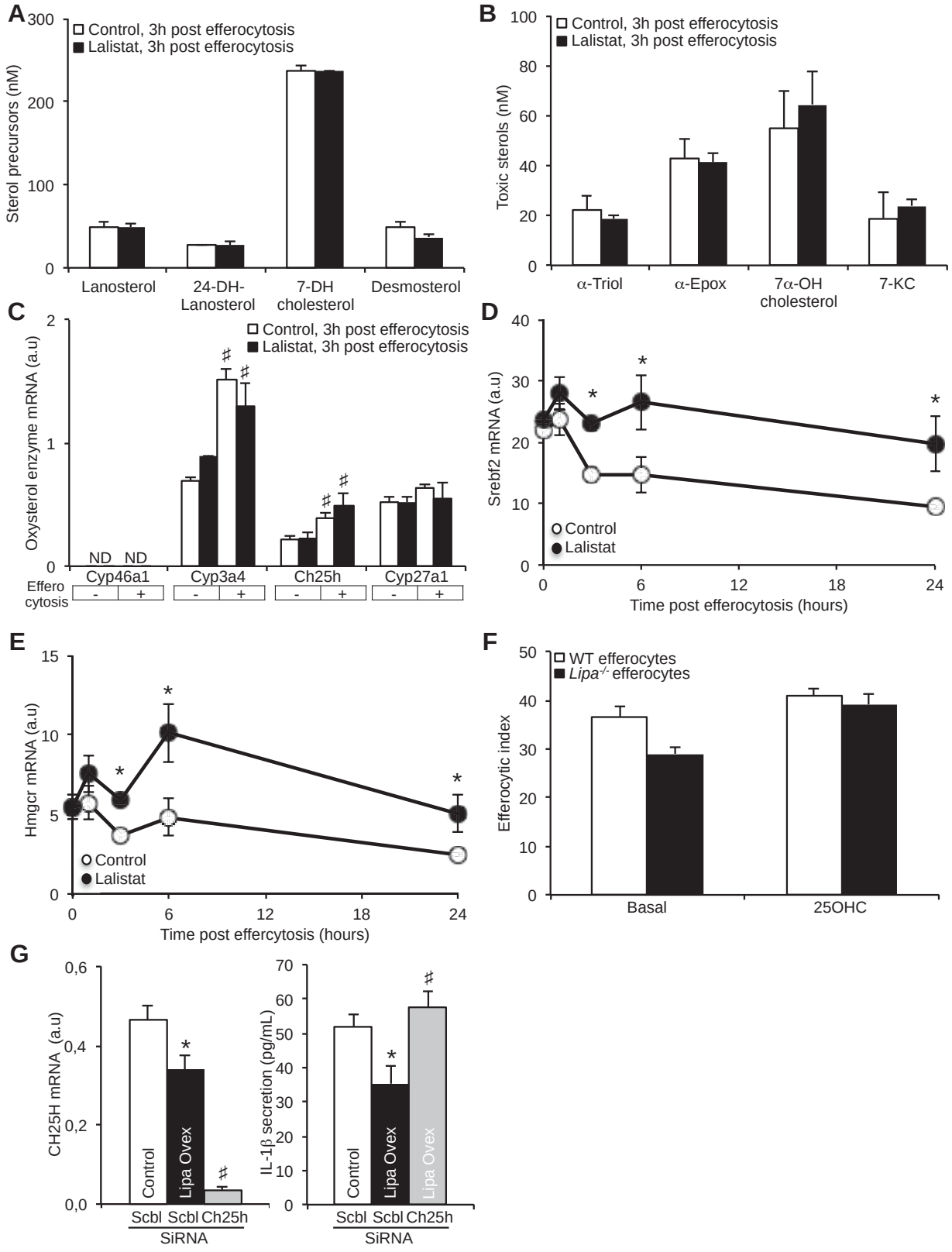

Supplemental Figure VI.

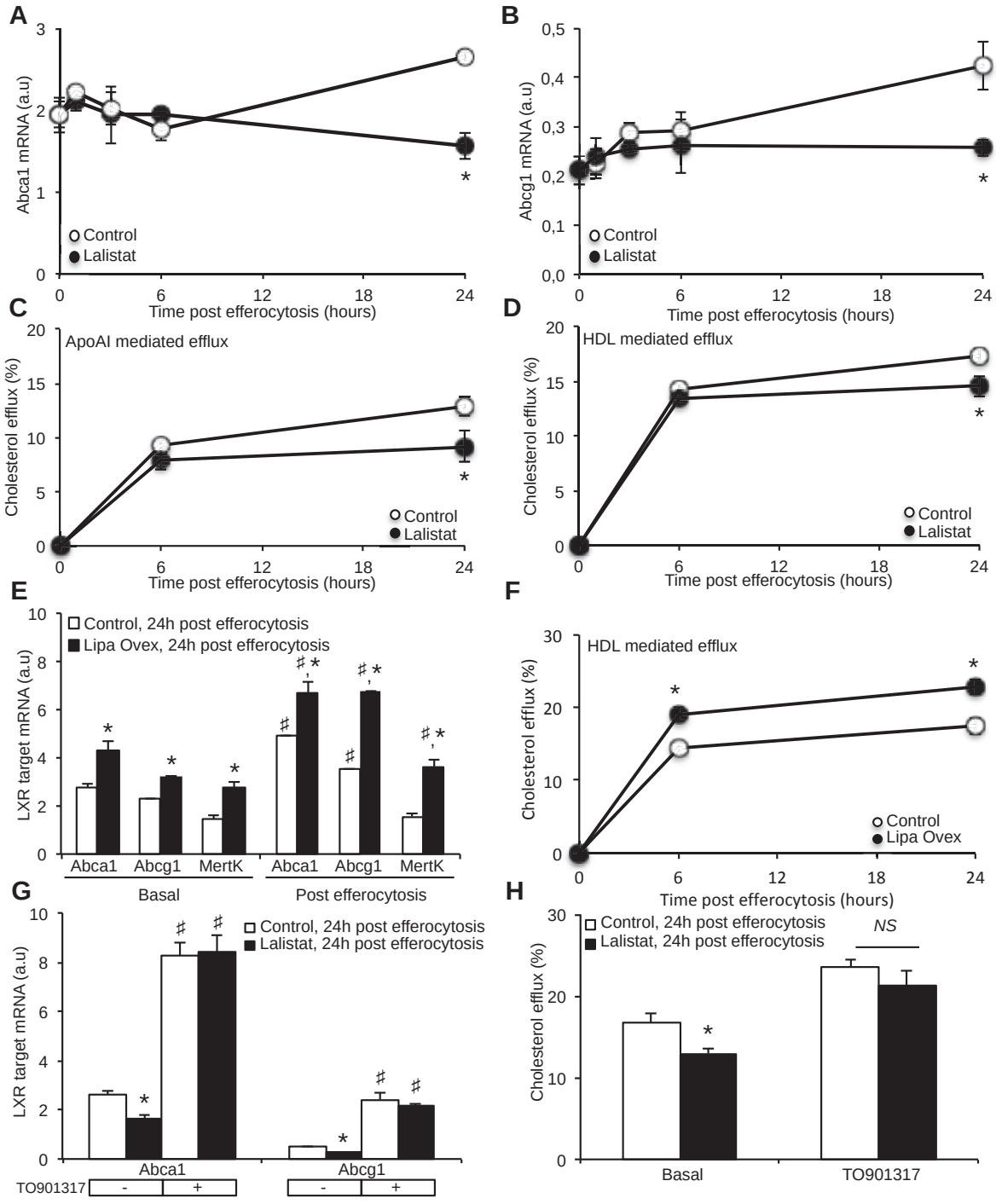

Supplemental Figure VII.

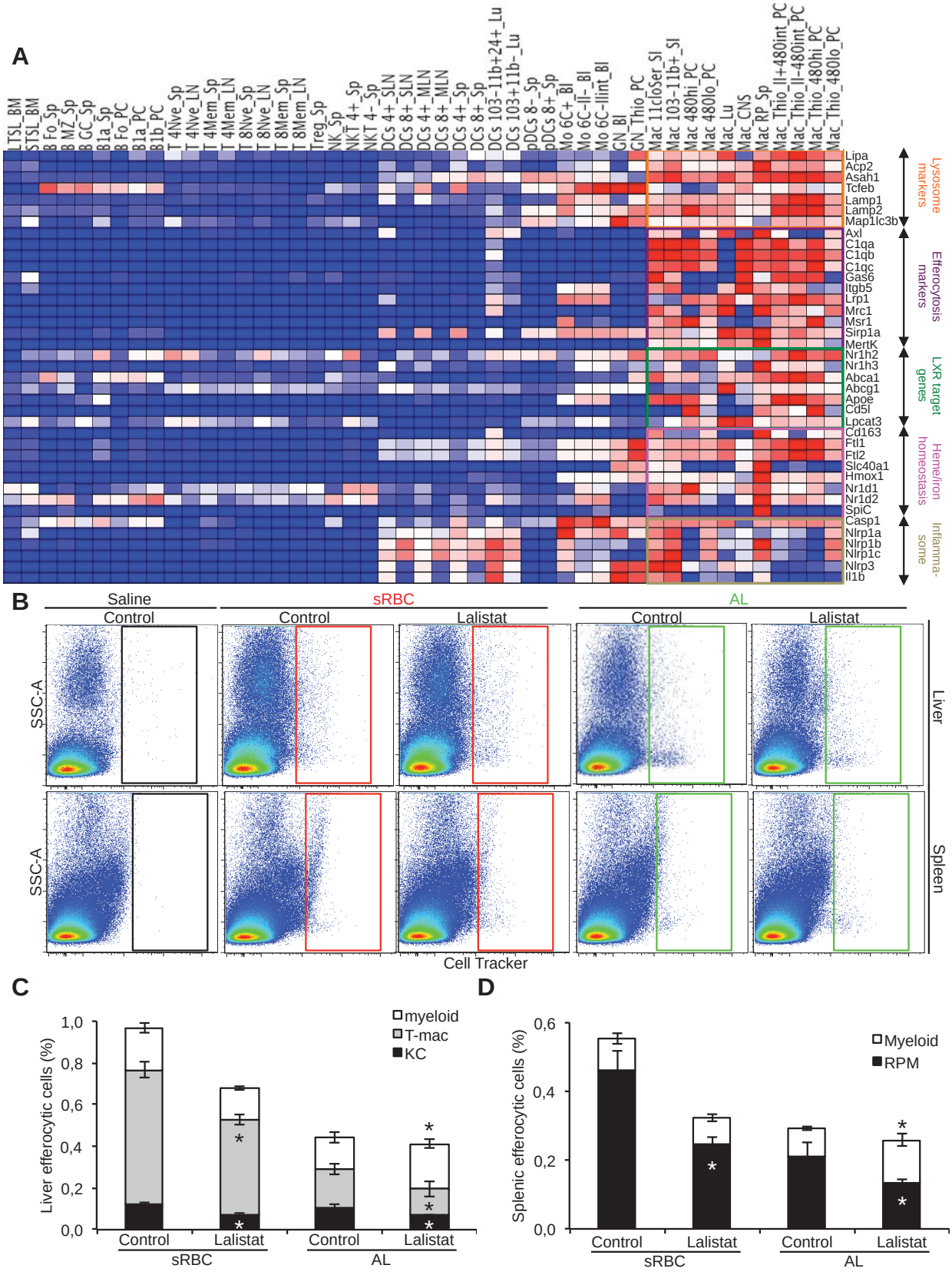

Supplemental Figure VIII.

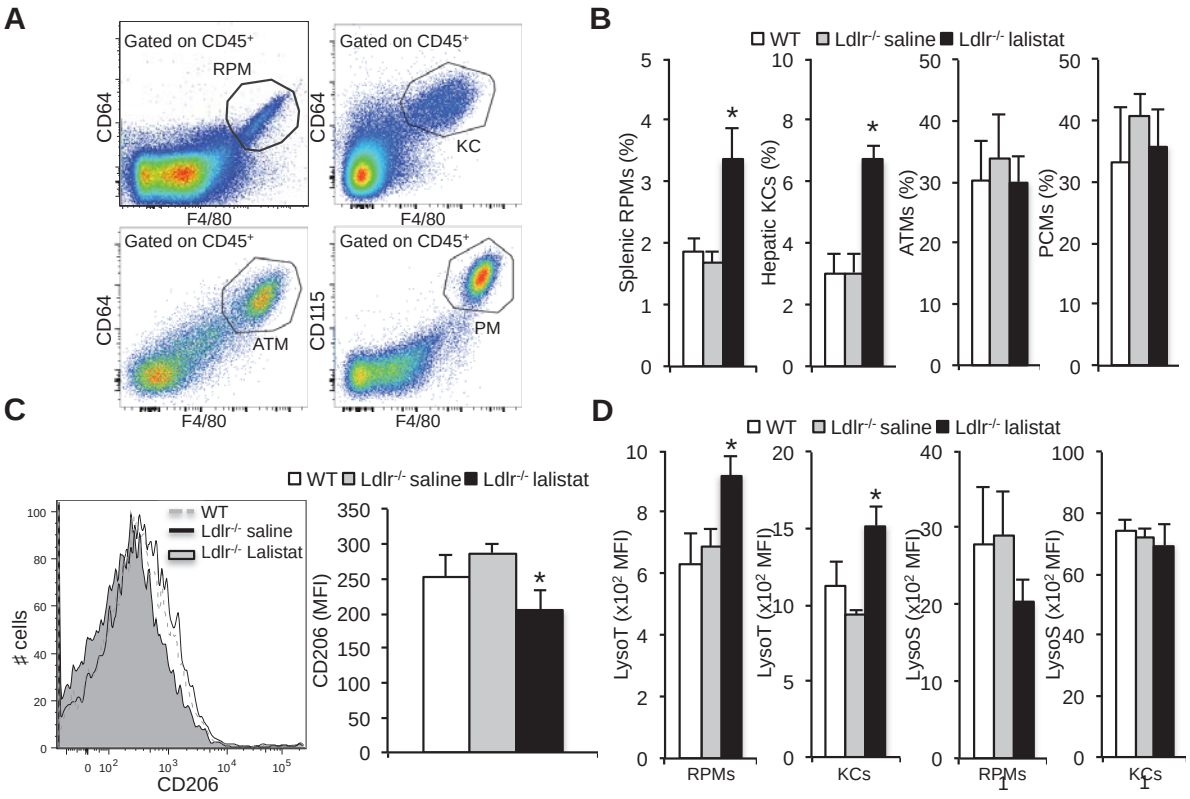

*** Long In Vivo Checklist**

Circulation Research - Preclinical Animal Testing: A detailed checklist has been developed as a prerequisite for every publication involving preclinical studies in animal models. ***Checklist items must be clearly presented in the manuscript, and if an item is not adhered to, an explanation should be provided.*** *If this information (checklist items and/or explanations) cannot be included in the main manuscript because of space limitations, please include it in an online supplement. If the manuscript is accepted, this checklist will be published as an online supplement. See the explanatory editorial for further information.*

This study involves use of animal models:

Yes

Study Design

The experimental group(s) have been clearly defined in the article, including number of animals in each experimental arm of the study.	Yes
An overall study timeline is provided.	Yes
The protocol was prospectively written	Yes
The primary and secondary endpoints are specified	Yes
For primary endpoints, a description is provided as to how the type I error multiplicity issue was addressed (e.g., correction for multiple comparisons was or was not used and why). (Note: correction for multiple comparisons is not necessary if the study was exploratory or hypothesis-generating in nature).	Yes
A description of the control group is provided including whether it matched the treated groups.	Yes

Inclusion and Exclusion criteria

Inclusion and exclusion criteria for enrollment into the study were defined and are reported in the manuscript.	N/A
These criteria were set *a priori* (before commencing the study).	N/A

Randomization

Animals were randomly assigned to the experimental groups. If random assignment was not used, adequate explanation has been provided.	Yes
Type and methods of randomization have been described.	Yes
Allocation concealment was used.	N/A
Methods used for allocation concealment have been reported.	N/A

Blinding

Blinding procedures with regard to masking of group/treatment assignment from the experimenter were used and are described. The rationale for nonblinding of the experimenter has been provided, if such was not performed.	Yes
Blinding procedures with regard to masking of group assignment during outcome assessment were used and are described.	Yes
If blinding was not performed, the rationale for nonblinding of the person(s) analyzing outcome has been provided.	N/A

Sample size and power calculations

Formal sample size and power calculations were conducted before commencing the study based on *a priori* determined outcome(s) and treatment effect(s), and the data are reported.	Yes
If formal sample size and power calculation was not conducted, a rationale has been provided.	N/A

Data Reporting

Baseline characteristics (species, sex, age, strain, chow, bedding, and source) of animals are reported.	Yes
The number of animals in each group that were randomized, tested, and excluded and that died is reported. If the experimentation involves repeated measurements, the number of animals assessed at each time point is provided is provided for all experimental groups.	Yes
Baseline data on assessed outcome(s) for all experimental groups are reported.	N/A
Details on important adverse events and death of animals during the course of the experiment are reported for all experimental groups.	N/A
Numeric data on outcomes are provided in the text or in a tabular format in the main article or as supplementary tables, in addition to the figures.	Yes
To the extent possible, data are reported as dot plots as opposed to bar graphs, especially for small sample size groups.	N/A
In the online Supplemental Material, methods are described in sufficient detail to enable full replication of the study.	Yes

Statistical methods

The statistical methods used for each data set are described.	Yes
For each statistical test, the effect size with its standard error and *P* value is presented. Authors are encouraged to provide 95% confidence intervals for important comparisons.	Yes
Central tendency and dispersion of the data are examined, particularly for small data sets.	N/A
Nonparametric tests are used for data that are not normally distributed.	Yes
Two-sided *P* values are used.	N/A
In studies that are not exploratory or hypothesis-generating in nature, corrections for multiple hypotheses testing and multiple comparisons are performed.	Yes
In "negative" studies or null findings, the probability of a type II error is reported.	N/A

Experimental details, ethics, and funding statements

Details on experimentation including formulation and dosage of therapeutic agent, site and route of administration, use of anesthesia and analgesia, temperature control during experimentation, and postprocedural monitoring are described.	Yes
Both male and female animals have been used. If not, the reason/justification is provided.	Yes
Statements on approval by ethics boards and ethical conduct of studies are provided.	Yes
Statements on funding and conflicts of interests are provided.	Yes

---

Date completed: 03/05/2018 13:28:32
User pid: 134917